Official journal of the JHL 2689-9620
www.light-am.com

Review Open Access

Imaging/nonimaging microoptical elements and stereoscopic systems based on femtosecond laser direct writing

Long Huang[1], Zhihan Hong[2], Qi-Dai Chen[3], Yong-Lai Zhang[3], Shaoqing Zhao[1], Yongjun Dong[1], Yu-Qing Liu[1,*] and Hua Liu[1,*]

Abstract

The development of modern information technology has led to significant demand for microoptical elements with complex surface profiles and nanoscale surface roughness. Therefore, various micro- and nanoprocessing techniques are used to fabricate microoptical elements and systems. Femtosecond laser direct writing (FsLDW) uses ultrafast pulses and the ultraintense instantaneous energy of a femtosecond laser for micro-nano fabrication. FsLDW exhibits various excellent properties, including nonlinear multiphoton absorption, high-precision processing beyond the diffraction limit, and the universality of processable materials, demonstrating its unique advantages and potential applications in three-dimensional (3D) micro-nano manufacturing. FsLDW has demonstrated its value in the fabrication of various microoptical systems. This study details three typical principles of FsLDW, several design considerations to improve processing performance, processable materials, imaging/nonimaging microoptical elements, and their stereoscopic systems. Finally, a summary and perspective on the future research directions for FsLDW-enabled microoptical elements and stereoscopic systems are provided.

Keywords: Femtosecond laser direct writing, Microoptical elements, 3D printing, Micro/nano fabrication

Introduction

Traditional macroscopic optical systems are usually composed of macroscopic optical elements, which have the problems of bulky volume, high energy consumption, and low design freedom[1–3]. By contrast, microoptical elements and stereoscopic systems with miniaturized sizes, integrated modules, diversified functions, and low power consumption show significant advantages in imaging (such as biomedical imaging, photonics chip imaging, and infrared imaging) and nonimaging (such as beam shaping, optical fiber and waveguide fabrication, and optical storage) applications[4–9]. With the development of modern information technology, increasing demand has been observed for microoptical elements and systems[10–14]. The demand for microoptical elements with complex surface profiles, nanoscale surface roughness, and more integrated optical systems has driven the development of various micro- and nanofabrication technologies[15–21]. Currently, the most common micro- and nanoprocessing technologies are electron beam lithography (EBL), nanoimprint, digital light processing (DLP)[22–25], direct ink writing (DIW)[26],

Correspondence: Yu-Qing Liu (liuyq@nenu.edu.cn) or Hua Liu (liuh146@nenu.edu.cn)
[1]Center for Advanced Optoelectronic Functional Materials Research, and Key Laboratory for UV-Emitting Materials and Technology of Ministry of Education, National Demonstration Center for Experimental Physics Education, Northeast Normal University, 5268 Renmin Street, Changchun 130024, China
[2]Wyant College of Optical Sciences, The University of Arizona, 1630 E. University Blvd, Tucson, Arizona 85721, USA
Full list of author information is available at the end of the article.

stereolithography (SLA)[27,28] and femtosecond laser direct writing (FsLDW)[29–31]. EBL uses electron-beam scanning to process polymers into delicate structures, typically with a resolution of 3–8 nm[32,33]. However, slow processing speed and high equipment costs have limited the widespread use of EBL. Nanoimprint can also achieve nanoscale resolution; however, it can only produce two-dimensional (2D) structures on flat surfaces, and processing three-dimensional (3D) structures is challenging. DLP has attracted considerable attention because of its rapid printing speed and micron-level molding accuracy[34–37]. However, the step effect between the layers leads to a rough surface in the processed structure, which seriously affects the imaging performance of the optical elements[38,39]. The processing resolutions of DIW and SLA are at the micron level and cannot meet the processing requirements of microoptical elements with nanometer-scale surface roughness[40–42].

FsLDW uses ultrafast pulses and ultraintense instantaneous energy of a femtosecond laser to process materials[43] and is used in various applications, including semiconductors, automobiles, biomedicine, microfluidics, and microoptics. Particularly in the field of micro- and nanooptical element and system processing, FsLDW shows various advantages compared to the aforementioned processing methods[44,45]. First, owing to its nonlinear multiphoton absorption characteristics, FsLDW exhibits processing accuracy beyond the diffraction limit[46]. It can process voxels smaller than 100 nm using sizeable numerical aperture (NA) objectives[47–49]. Moreover, the ability of femtosecond lasers to penetrate surfaces for 3D processing enables the fabrication of complex microoptical elements and systems[50–52]. Processing optical elements directly on the surface of devices such as optical fibers and sensors is also possible. In addition, FsLDW is a cold-processing technique owing to its short pulse duration and small area of thermal damage. Finally, FsLDW is universal for processable materials and used to process various materials, including polymers, metals, ceramics, and hard materials (such as glass and sapphire)[53]. Single-point scanning of FsLDW is less efficient; however, it can be improved by combining FsLDW with other processing methods[54,55]. The FsLDW technology has recently shown tremendous development prospects for fabricating accurate 3D microoptics[56,57]. In this paper, we review recent progress in fabricating microoptical elements and systems using FsLDW. Three typical femtosecond laser processing principles, namely, two-photon polymerization (TPP)[58,59], femtosecond laser ablation (FLA), and femtosecond laser modification (FLM)[60,61], are introduced in detail. Then, we propose design considerations for fabricating microoptical elements, including improving the processing performance and processable materials. In terms of applications, various imaging/nonimaging microoptical elements processed using FsLDW and their stereoscopic systems have been discussed. Finally, we discuss the future development trends of FsLDW-enabled microoptical elements.

Technologies of FsLDW

Fig. 1a shows a typical femtosecond laser processing system. FsLDW is classified into three typical methods: TPP[62,63], FLA, and FLM. These three methods are based on different materials and are suitable for various applications. This section focuses on the processing principles of the three methods.

Processing principle of TPP

TPP is a unique photopolymerization micro-nano fabrication technique that utilizes the nonlinear effect of two-photon absorption to prepare 3D microstructures with characteristic dimensions beyond the diffraction limit[64]. In the single-photon absorption process, materials can only absorb a single photon with energy larger than their bandgap, achieving a transition from the ground state to the excited state. By contrast, when the incident light has a sufficiently high intensity, such as a femtosecond laser, materials can absorb two or more photons simultaneously to achieve an energy level transition. The energy of the femtosecond laser pulses conformed to a Gaussian distribution, which implies that the energy was the highest at the center of the spot and gradually decreased as the distance from the spot increased (Fig. 1b). Based on this theory, only the energy of a small area around the center of the spot can generate two-photon absorption. Therefore, processing accuracy with a sub-diffraction limit can be obtained using TPP[65]. In addition, TPP is a typical nonlinear process, and the probability of its occurrence is proportional to the square of the laser power[66,67]. Two-photon absorption can only be induced when the laser intensity exceeds a specific critical value, that is, the energy threshold. Leveraging this characteristic, the reaction area can be limited very near the focal point inside the material by focusing the femtosecond laser to realize true 3D processing.

Processing principle of FLA

The FLA is realized using the ultrahigh peak intensity and ultrashort pulse width of a femtosecond laser. For long-pulse lasers (e.g., >1 ns), the processing material has sufficient time to melt within the focused volume after being heated[68]. Meanwhile, the heat diffuses into the surrounding area, forming a thermal damage zone and resulting in poor processing quality. By contrast, when

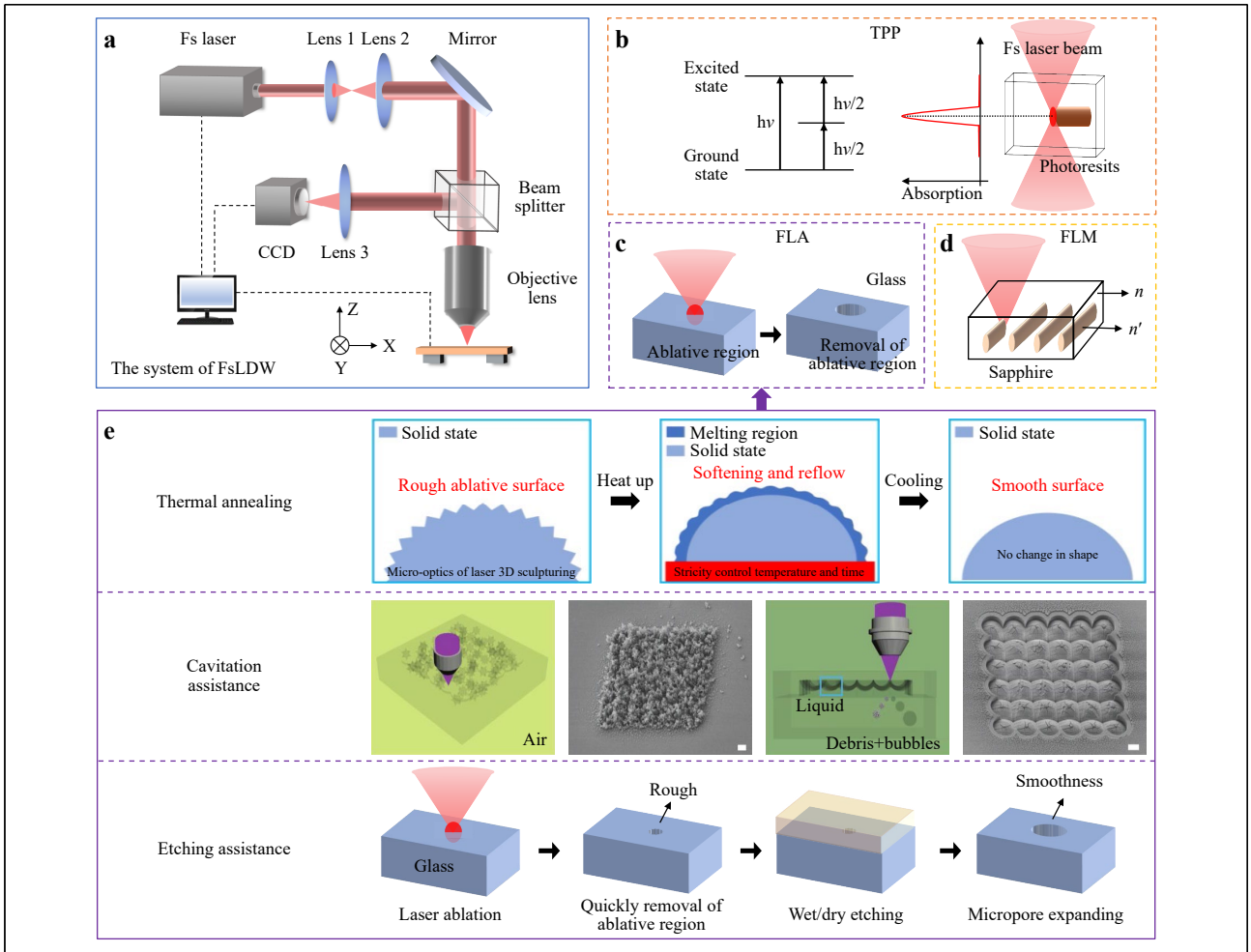

Fig. 1 Diagram of the femtosecond laser system and processing principle. **a** Diagram of the FsLDW system. The principle of **b** two-photon polymerization (TPP), **c** femtosecond laser ablation (FLA) and **d** femtosecond laser modification (FLM). **e** Assisted methods for FLA [obtained from ref. 71].

processing with ultrashort continuous femtosecond laser pulses, the pulse width is considerably shorter than the thermal diffusion time generated by coupling electrons and phonons. Therefore, the femtosecond laser can induce the rapid ionization of materials and produce plasma with high temperature, pressure, and density, thereby realizing the nonthermal ablation of materials and forming an ablation point depression (Fig. 1c). The nonthermal processing characteristic of a femtosecond laser ensures high-precision and high-quality processing of the material surface and maintains the stability of the optical, mechanical, and thermal properties of the material[69,70].

To smooth the surface of an ablative machining structure further, combining auxiliary methods is necessary. The technologies of thermal annealing assistance[71–74], cavitation assistance, and etching assistance (wet etching and dry etching[75,76]) are shown in Fig. 1e. Thermal annealing is typically used for amorphous materials such as glass[77]. Glass has no fixed melting point, and its transformation from solid to liquid occurs within a specific temperature range. By strictly controlling the thermal annealing temperature (⩾1100 ℃) and time, only the glass surface is directly melted, and internal softening is minimized. The increase in the molecular kinetic energy on the surface, together with the microflow owing to the surface tension effect, produces a smooth surface similar to a liquid surface. Consequently, the surface quality significantly improved after cooling. The cavitation-assisted FLA is displayed in Fig. 1e (middle). The samples were covered with a liquid-filled recess to form an airtight environment. A femtosecond laser penetrates the material and focuses on the interface between the material and liquid. The ultrahigh peak power at the laser focus causes ablation of the material and cavitation of liquid bubbles[78]. The cavitation bubbles then pulsate and collapse on the sample surface, applying pressure to the ablative area, which can clean the

ablated debris, resulting in a smooth surface[79]. Etching-assisted technology mainly consists of two steps: First, FLA is used to prepare the structure, and then, a suitable etching solution is selected to etch the processed area, reducing the surface roughness[80]. The surface roughness of an ablative structure is significantly reduced by using several auxiliary methods.

Processing principle of FLM

When a femtosecond laser is focused within a densely structured material, certain properties of the material in the focal region change after absorbing the laser energy; this process is defined as the FLM[81–83]. FLM does not change the shape of the material and is a unique processing mode of the femtosecond laser. After absorbing energy, electrons in the processing area are transferred to the lattice, and different types of modified structures are produced during this process. According to current research, FLM includes changes such as permanent refractive index changes, nonlinear coefficient changes, and fluorescence signal changes[84–86]. When the laser pulse energy reaches the modification threshold of the material, an isotropic refractive index change is generally formed within the material (Fig. 1d). The refractive indices of most materials increase after modification. When the pulse energy is further increased, a significant birefringence phenomenon occurs in the modified regions of materials such as quartz and borosilicate glass because of the formation of a lamellar nanogrid structure inside the material. The change in the refractive index caused by the FLM can be applied to the processing of 3D microoptical elements. The fabrication of optical devices using nonlinear photonic crystals is an important topic of research. FLM can modulate second-order nonlinear optical coefficients in the 3D space of crystals with excellent nonlinear optical properties (such as lithium niobate) and obtain 3D nonlinear optical elements[87,88]. Therefore, changes in the fluorescence signals (photochromism or photobleaching) of transparent materials by FLM can be used for 3D optical storage. Compared to traditional surface-embossed elements, 3D optical elements processed inside a hard material by FLM exhibit unique advantages in terms of wear resistance and stability.

Design considerations for fabricating imaging/nonimaging microoptical elements

In addition to selecting appropriate processing methods, other important design factors must be considered, such as strategies for achieving high efficiency, methods for converting data points from 3D models, and materials for microoptical elements. The following section will discuss these three aspects.

Strategies for achieving high efficiency

Generally, FsLDW uses a point-by-point processing method with a very small voxel, which is time-consuming when processing 3D structures with millions of pixels[89,90]. The single-point scanning mode of femtosecond lasers can no longer satisfy the requirements of efficient processing. Therefore, developing various methods to improve processing efficiency is essential.

High-speed voxel-modulation laser scanning (HVLS)

The energy of the laser focus controls the size of the processing voxels. On the one hand, smaller voxels can be obtained to fabricate high-precision 3D structures by reducing the energy of the femtosecond laser. However, this requires extended processing time. On the other hand, high exposure energy leads to an increase in voxel size, which significantly reduces the processing time. However, this results in high surface roughness. Therefore, by taking advantage of small and large voxels, different voxel sizes can be combined for processing to meet complex requirements. For example, large voxels are used to fabricate a microoptical element base quickly, and small voxels are used to obtain a 3D structure with a smooth surface, as shown in Fig. 2a[91]. Two-photon grayscale lithography is a voxel modulation method that quickly and accurately modulates the irradiation dose through a single scanning plane[92,93]. This technique provides the high precision required for high-speed printing and manufacturing complex micropatterned structures.

Multiple-spot parallel processing (MSPP).

In addition to increasing the voxel size, the processing efficiency can be improved by increasing the number of femtosecond laser spots[94–98]. For example, Yang et al. established a multifocus TPP system based on a spatial light modulator (SLM)[99]. In their system, the laser beam completely irradiated the SLM with only phase modulation after passing through the beam expander. When computationally generated holograms (CGH) were loaded onto the SLM, the gray levels on the computational holograms modulated the 0–2π phase shift of the corresponding laser beam. Consequently, the femtosecond laser beam reflected from the SLM is modulated into multiple beams with a specific distribution, and multiple laser beams were subsequently focused on the platform to fabricate the structures. Maibohm et al. used diffractive optical elements (DOEs) to produce nine parallelized multibeamlets. The experimental setup is shown in Fig. 2b[96]. SLMs (such as microlens arrays (MLA) or DOEs) are introduced into TPP manufacturing systems through which the femtosecond laser beam can be split into

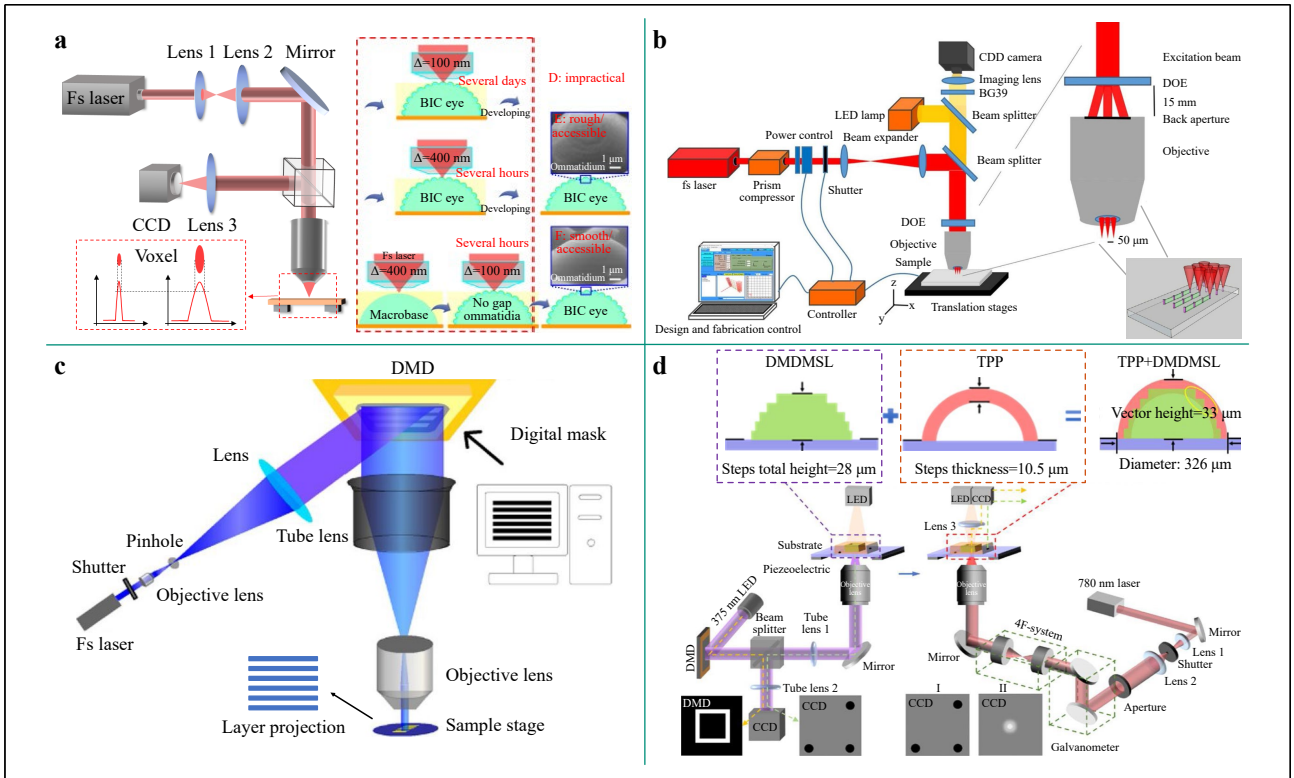

Fig. 2 a Processing method of high-speed voxel-modulation laser scanning (HVLS) [obtained from ref. 91]. **b** System of multiple-spot parallel processing (MSPP) with diffractive optical elements (DOEs) [obtained from ref. 99]. **c** Processing system of maskless optical projection nanolithography (MLOP-NL) based on digital mirror device (DMD) [obtained from ref. 102]. **d** Hybrid 3D printing method and system [obtained from ref. 105].

tens or even hundreds of light points[100,101]. These methods enable parallel processing of the femtosecond laser to improve the processing efficiency.

Maskless optical projection nanolithography (MLOP-NL)

Maskless optical projection lithography is a crucial technology in micro- and nanoscale graphics. Combining it with a femtosecond laser changes the point exposure mode to the planar exposure mode, significantly improving the processing efficiency. Liu et al. proposed and demonstrated an MLOP-NL system (Fig. 2c) for efficient cross-scale patterns[102]. The essential component of this system is a digital mirror device (DMD). The DMD modulates the laser beam by controlling the micromirror array, which produces a target exposure pattern for each layer. The MLOP-NL technology not only dramatically improves efficiency but also provides a powerful tool for fabricating multiscale integrated microsystems. Notably, the diffraction of the incident laser on the DMD and gap between the micromirrors results in significant energy loss, which requires a high laser power.

Hybrid 3D printing method

The collaborative use of multiple 3D printing technologies can improve processing efficiency and achieve cross-scale processing[103,104]. For example, Tan et al. combined the advantage of TPP and DMD micro stereolithography (DMDMSL) (TPP-DMDMSL) for hybrid 3D printing (Fig. 2d)[105,106]. The TPP system can produce voxels with a diameter of 400 nm; however, its processing efficiency is low. Conversely, the processing speed of the DMDMSL system is fast, but the minimum resolution is only ~1 μm. The two systems were used for different parts of the 3D structures with different precision requirements to balance the processing time and resolution. To fabricate the aspheric lens, the TPP method was used for the high-precision processing of the surface, whereas the internal steps of the lens without high precision were processed using DMDMSL. Because the two systems are independent, they mark the substrate with circular marks to enable the two systems to process on the same substrate. High-precision positioning was performed by identifying circular marks in the CCD. Overall, TPP-DMDMSL combines the high resolution and superior design flexibility of TPP with the rapid processing capabilities of DMDMSL for efficient, high-precision printing. Table 1 provides a comparison of the processing methods used in this study.

Table 1 A comparison of various FsDLW technologies.

Technology		Light source	Energy intensity	Spatial resolution	Characteristic	
Basic methods	TPP	Fs laser	Low	10 nm-μm[145]	Nonlinear effect	Single point scanning, low efficiency
	FLA	Fs laser	High	250 nm-μm[70]	Non-thermal ablation	
	FLM	Fs laser	Medium	~1 μm[85]	Processed inside the hard material	
Highly effective strategies	HVLS	Fs laser	Low	100 nm-400 nm[91]	Voxel-modulation, bigger voxels enhance efficiency	
	MSPP	Fs laser	Medium	90 nm-μm[263]	Multibeam processing, parallelized processing enhance efficiency	
	MLOP-NL	Fs laser	High	32 nm-μm[102]	Planar exposure mode besed on DMD	High processing efficiency, can achieve cross-scale processing
	TPP-DMDMSL	Fs laser and LED	Low	500 nm-μm[105]	Multiple 3D printing technology synergy	

Notably, the obtained spatial resolution varies depending on the processed material and the projection lens magnification of the femtosecond laser processing system.

Method of transforming a 3D model into data points

Before processing, the 3D model must be translated into individual data-point coordinates, each of which is the location of a voxel[107,108]. During TPP, the femtosecond laser performs point-by-point processing according to the data points, and the processing area is photopolymerized to form a 3D structure. Because of its ablative properties, the data points used for processing in FLA are from structures that need to be removed. For the FLM, the area processed according to the data points was the laser-modified structural area. This section introduces a method for transforming a 3D model into data points. Notably, given the various efficiency improvement methods in section of "Strategies for achieving high efficiency, the methods of transforming the 3D model into data points need to be adjusted accordingly.

Transforming all the 3D models into data points

In general, we convert the entire structure of the printed model into data points. During the conversion, the 3D model must be converted into a layer-by-layer 2D plane structure, where each layer is a single 2D data point (i.e., X and Y coordinate points). We also need to get the Z coordinate of each 2D plane structure, which is called slicing. The slicing process generally uses the equal-height slicing method[109,110], which refers to an equal distance between each layer of a 3D model. However, for 3D curved microstructures (such as optical lenses and spherical microstructures), the thickness of the slice is a key factor that determines the surface quality. An image of the lens surface obtained by equal-height slicing with a layer spacing h of 100 nm is shown in Fig. 3b. Apparent solenoid traces are observed owing to the lateral offset of

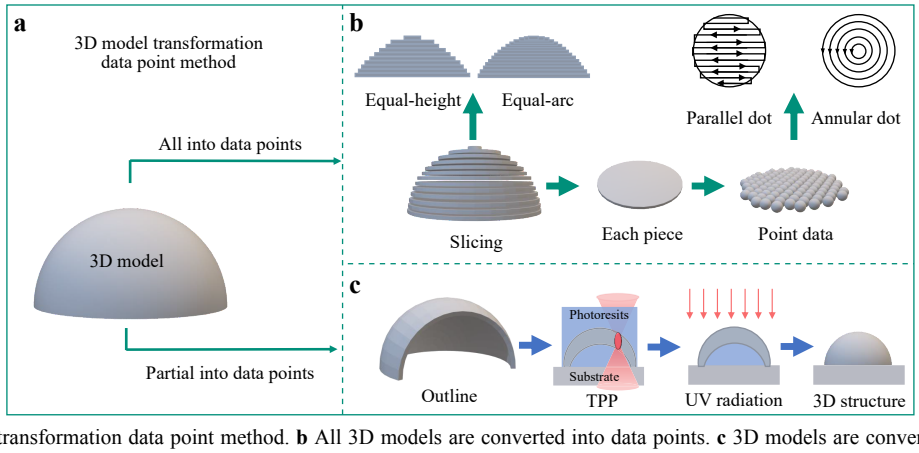

Fig. 3 a 3D model transformation data point method. **b** All 3D models are converted into data points. **c** 3D models are converted into data points partially.

the voxel position, particularly at the top of the lens. This lateral offset has a significant effect on the roughness of the lens surface. Therefore, equal-height slicing is not an effective method for dealing with 3D microstructures of lenses. An equal-arc slicing method has been proposed to compensate for the large offset of voxels in the equal-height slicing method[111–113], which implies that the layer height $\Delta h = \Delta L \times \sin\theta$ is variable. Δh depends on the arc length ΔL and sloping angle . A microlens with a smooth surface is obtained by selecting an appropriate arc for the isoarc slicing.

Then, we transformed each 2D slice into a series of points containing X and Y coordinates[114,115]. The 2D slices are generally transformed into parallel point coordinates that are suitable for most microstructures. However, because each layer of the microlens exhibits a circular structure, the lines formed by the coordinates of parallel points not only distort the outline of the circle but also create some protrusions on the edges of the lens surface. Therefore, to obtain optical elements with smooth edges, annular point coordinates are generally chosen to ensure circular symmetry and radial consistency of the lens.

Transforming a portion of the 3D models into data points

To obtain a reduced number of data points, the 3D model can be partially (i.e., the contour) converted into data points[116,117] (Fig. 3c). During TPP, the voxel size can be controlled by changing the laser power or scanning speed to create a shell with sufficient mechanical strength[114]. The unpolymerized portion of the outer layer of the contour was then removed by developing. Finally, the inner part of the contour is irradiated with UV light to obtain a completely polymerized structure. The fabrication of the shell, development, and post-processing with UV light significantly reduced the processing time. However, the contour scanning method requires a processed material with high mechanical strength. Otherwise, the development causes the collapse of the polymerization contour, resulting in processing failure. For FLA processing, detaching the part outside the target structure is also possible by processing only the contour data points.

Two types of data point conversion methods are available for single-point scanning processing, which are the most basic data point conversion methods. To improve the efficiency of the different processing methods mentioned in section of “Strategies for achieving high efficiency”, we need to improve the data point conversion methods correspondingly. For example, we need to modify the distance between voxels for HVLS. In the case of the MSPP, the SLM needs to be controlled to generate multiple focuses. For the MLOP-NL, the data points must be modified to the plane projection data of the DMD. In the hybrid 3D printing method, models and data points must be split.

Processing materials for FsLDW

Materials suitable for optical element processing can also be categorized according to the three optical element processing methods in FsLDWs. The first is photopolymerization materials applicable to TPP, which mainly include polymeric materials and organic-inorganic hybrid materials[118]. Polymeric materials include resins[119–123], polydimethylsiloxane (PDMS)[124], and proteins[125,126]. Organic–inorganic hybrid materials include silicon nanocomposite[127–129], sol–gel glass[130,131], and polyhedral oligomeric silsesquioxane (POSS) glass materials, which can form glass after heat treatment[132,133]. Second, hard and brittle materials with excellent stability and optoelectronic properties are suitable for FLA, including crystalline (sapphire and silicon) and noncrystalline (glass) materials. The materials used for FLM include glass, crystalline materials, graphene, and hydrogels, which partially overlap with the materials used for FLA. A partial overlap occurs between photopolymerized and ablative materials, such as certain photoresists and other polymeric materials that can be processed by both photopolymerization and laser ablation. However, the ablation process usually results in high surface roughness, which cannot meet the high-precision requirements of optical elements. By contrast, the structures obtained by photopolymerization exhibit smoother surfaces with smaller voxels[134,135]. Therefore, overlapping materials are primarily processed using photopolymerization. The classification and corresponding auxiliary processing methods for the processed materials are shown in Fig. 4.

Photopolymeric materials

Various photopolymerization materials are suitable for TPP. Several resin materials can be self-configured, the advantage of which is that the ratio of each part of the material can be adjusted according to the device requirements to obtain the best printing results. In addition, mature commercialized photoresists and other resin materials can be purchased. The commonly used photoresists are the SU-8 series[125] (manufacturer Microlithography Chemical) and IP series[120]. SU-8 is a near-UV photoresist based on an epoxy resin (from the rubber industry), which exhibits excellent imaging properties. Owing to its low absorption in the wavelength range of 365–400 nm, each layer of SU-8 can obtain uniform exposure. Therefore, it can process thick-film structures with vertical sidewalls and high aspect ratios. IP series photoresists have a wide variety of IP series

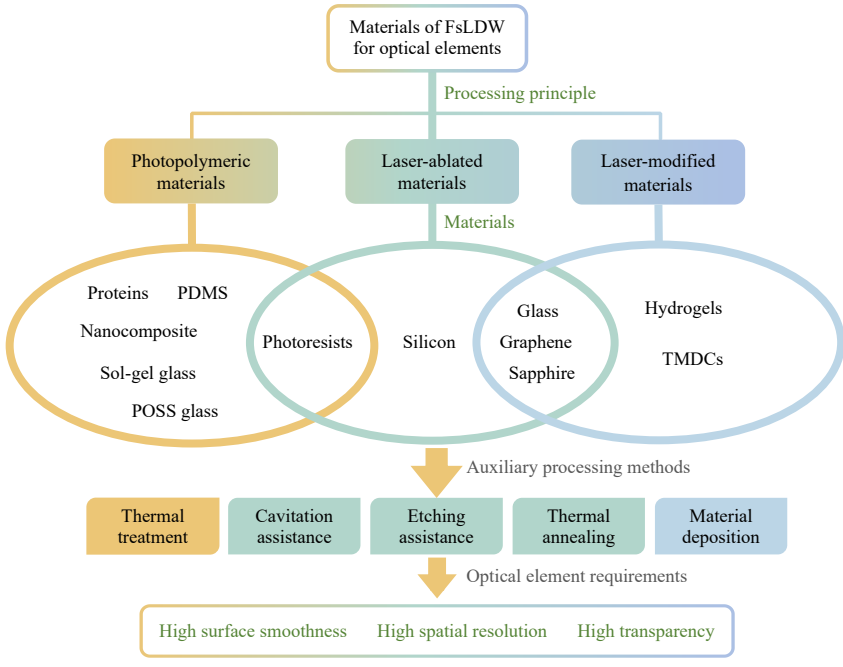

Fig. 4 Various materials for fabricating microoptical elements using FsLDW and their auxiliary processing methods.

photoresists, mainly IP-S and IP-n162. The optical, mechanical, electronic, and biological properties of these photoresists were engineered to make them suitable for optical, optoelectronic, and biomedical applications.

Commercial bovine serum albumin (BSA, aqueous solution) was used to process the optical microdevices. When methylene blue is used as a photosensitizer, the absorbed laser energy is transferred to ground-state oxygen, forming reactive oxygen species such as singlet oxygen. Singlet oxygen can easily catalyze the inter- or intramolecular covalent crosslinking of oxidizable protein residues (such as Tyr, Trp, and His), forming a 3D protein microhydrogel[125,126]. After processing, proteins at higher concentrations (400–500 mg/mL) can achieve a more robust mechanical structure. The natural structure of a protein undergoes reversible conformational isomerization at different pH values. Microoptical elements processed with proteins have flexibility and extensibility, as well as good biocompatibility and biodegradability.

PDMS exhibits 100% light transmittance and is an ideal hydrophobic silica gel material for processing optical elements[124,136]. PDMS is nontoxic, odorless, physiologically inert, chemically stable, electrically insulating, weather-resistant, soft, and can be processed into soft lenses. Moreover, PDMS is highly sensitive to organic solvents, and most organic solvents diffuse into PDMS materials, leading to material expansion. Solvent-tunable PDMS microlenses are fabricated by exploiting the solvent responsiveness.

Some of the aforementioned soft materials have poor robustness and are unsuitable for use in extreme environments (such as strong acids, strong bases, and high temperatures). Hard materials such as quartz glass are the materials of choice for several high-performance elements in optics because of their high optical transparency and high thermal, chemical, and mechanical stability[137]. Fused silica microstructures are particularly attractive for optical and biomedical applications. Fused silica glass can be fabricated by firing some organic-inorganic hybrid materials. Three major types of organic–inorganic hybrid materials, including silica nanocomposites, sol–gel glass, and POSS glass materials, can be processed into glass by TPP and heat treatment. The first type is a mixture prepared by adding silica nanoparticle fillers to photopolymer precursors[127,138,139]. Photopolymerization precursors generally consist of two main components: small-molecule polymeric monomers and large-molecule crosslinkers. On the one hand, polymeric monomer solution allows the dispersion of large amounts of silica nanoparticles, while crosslinker can provide more chemical bonds for photopolymerization. By contrast, the polymeric monomers and crosslinkers exhibit different refractive indices. By adjusting the ratio in the solution, the overall refractive index can be made very close to that of silica. This reduces the scattering of light spots during processing, thereby improving the processing resolution. After curing

by TPP and thermal degreasing and sintering (>1100 ℃), silica nanocomposites can be transformed into fused silica glass, achieving a resolution of several hundred nanometers and a surface roughness of several nanometers[140]. Glass ceramics are formed from silica nanocomposites at precisely controlled temperatures (~1200 ℃) during sintering, which exhibit superior optical properties compared to ordinary glass materials, such as better robustness and lower scattering[141,142].

Unlike silicon nanocomposites, sol–gel glass materials do not require such high heat treatment temperature[130,143,144]. The sol–gel method uses inorganic salts containing silica as precursors, which are then gradually gelated through hydrolytic condensation. Finally, sol–gel glass materials (also known as liquid glass) were obtained after post-treatment and drying. Because the inorganic silica filler is introduced at the molecular scale by mixing the precursors, it allows the incorporation of silicon groups to control the homogeneity of the material better; thus, the particle cluster problem does not arise[130]. In addition, these precursors contain a photopolymerizable fraction (acrylate or epoxy resin). The sol–gel material was photocured using TPP to form a 3D structure. Then, it was degreased and sintered at 600 ℃. 3D structures with glass as the main body can be formed after cooling. Owing to the low heat-treatment temperature, sol–gel materials can be used to fabricate structures on the surface of devices that are not resistant to high temperatures. With the continuous development of sol–gel glass materials, further reducing the processing temperature and broadening the application scenarios is possible[145].

Another material that can be converted into fused silica at low temperatures (650 °C) is POSS glass[145,146]. The POSS glass consists of three components: 89 wt% acrylate-functionalized POSS monomer, 9 wt% trifunctional acrylic monomer, and 2 wt% photoinitiator of the α-aminoketone family. POSS is an organic–inorganic hybrid polymer consisting of a caged silicon–oxygen framework[147,148]. When sintered into a solid, POSS exhibits a better high-temperature resistance and robustness than most pure organic polymers. Long-armed, branched trifunctional acrylic provides important resilience against cracking, which is the key to printing structures with sufficiently dense silica-oxygen nanoclusters at a low temperature (650 °C). Furthermore, the viscosity of the resin can be regulated by varying the concentration of the trifunctional acrylates. The photoinitiator exhibited a high quantum yield for generating free radicals when excited at the 780 nm wavelength of the TPP system, thereby facilitating efficient polymerization of the materials. Overall, POSS glass materials exhibit excellent optical properties, mechanical elasticity, ease of processing, and high spatial resolution (down to 10 nm), which are suitable for the micro- and nano-3D printing of optical elements.

Laser-ablated material

Hard and brittle materials are also known as difficult-to-process materials, and their complex, brittle, and stable characteristics render fine processing much more complicated than that of ordinary materials[75,149]. Moreover, hard and brittle materials contain many material systems, and materials composed of different atoms exhibit significant differences in their physical and chemical properties. Other micro- and nanoprocessing techniques are challenging to apply to hard, brittle materials. Owing to the instantaneous high-intensity energy of the femtosecond laser, high-precision machining of hard and brittle materials can be achieved using FLA combined with several auxiliary methods in section of "Processing principle of FLA". Graphene oxide[150–152], optical glass[137,153,154], and crystals (such as sapphire [71,155] and silicon[146,156–158]) are the most widely used laser-ablative materials. These materials have excellent physical and chemical stabilities, including high hardness, high-temperature resistance, and corrosion resistance, and are widely used in extreme fields, such as the military and aerospace industries. They also have critical applications in microoptics and microelectronics, owing to their broad spectral transmittance, nonlinear optics, and other optoelectronic properties. Their combination of functionality and stability make them ideal materials for preparing micro- and nanooptical devices. For instance, except for diamonds, sapphire is the hardest natural mineral on Earth. Sapphire glass has excellent thermal properties, infrared transmission properties, and good chemical stability. Therefore, it is often used to fabricate optical elements and infrared-transparent optical windows and is widely used in infrared and far-infrared military equipment. Graphene is a novel material composed of carbon atoms arranged in a tightly packed single layer with a 2D honeycomb lattice structure that exhibits exceptional optical, electrical, and mechanical properties. Graphene is one of the most robust materials and is ductile and bendable. It holds significant potential for applications in micro- and nanoprocessing, materials science, energy, and biomedicine.

Laser-modified materials

Some laser-ablative materials such as glass, crystals, and graphene oxide[82,150] can also be used as laser-modified materials. Glass and crystalline materials exhibit good light transmission, and FLM can change their refractive indices, absorption coefficients, nonlinear optical sensitivities, and crystal structures[159]. Graphene oxide turns into reduced

graphene oxide under laser irradiation, and its optical properties significantly change during this process[160]. The optical reduction also results in much higher refractive index modulation (Δn of ~0.8) than conventional optical materials[161]. 2D layered materials generally refer to graphene and transition metal dichalcogenides (TMDCs) MX_2, where M is a transition metal atom (such as Mo and W), and X is a chalcogen atom (S, Se, or Te)[162–165]. Nanoparticles can be generated in single-layer TMDC crystals using femtosecond lasers to obtain amplitude or phase modulation by strong scattering of incident light[166]. 2D layered materials with sufficient phase or amplitude modulation can be processed into ultrathin lenses that can reach the thickness of a single atom[167].

In addition to the aforementioned materials, which can be directly fabricated into optical elements after modification, some materials, such as hydrogels, require post-treatment after modification. Femtosecond lasers can alter the polymer network of polyacrylate–polyacrylamide hydrogels in pure water, thereby reducing scaffold density and improving the ability to form hydrogen bonds[168]. Hydrogels can trap various materials through different interactions, including hydrogen bonds, charge effects, or dense scaffolds[169,170]. Therefore, various materials, such as metals, 2D materials, molecular crystals, semiconductors, biomaterials, and fluorescent substances, can be assembled onto hydrogels to form 3D structures. Moreover, to achieve processing resolutions below the diffraction limit (20–35 nm), pretuning the properties of the patterned gel before material deposition is necessary.

Imaging/non-imaging micro-optical elements

Owing to the aforementioned processing advantages, FsLDW technologies are widely used to fabricate various imaging/nonimaging microoptical elements. Microoptical elements are categorized into refraction, reflection, diffraction, and hybrid-principle microoptical elements according to their control capabilities over light, each of which can be further divided into imaging/nonimaging microoptical elements. In this section, we provide a detailed description of the microoptical elements.

Microoptical elements based on the principle of refraction

Refractive microoptical elements (such as microlenses and arrays) are widely used in various microoptical systems[171–173]. As an important type of refractive microoptical element, microlenses play an irreplaceable role owing to their small size, light weight, and excellent optical properties, particularly in the fields of beam shaping and imaging[174,175]. Xu et al. used TPP and SU-8 to process a concave–convex microlens (CCML) consisting of two different high-curvature surfaces[176], as shown in Fig. 5a. The CCML provides greater design flexibility and significantly enhances the optical performance, including aberration reduction. Sun et al. used bovine serum albumin (BSA) to process protein microlenses (Fig. 5b)[126]. When the protein microlens is stimulated by chemical signals, the microstructures exhibit rapid and reversible expansion and contraction. Thus, the focal length of the fabricated microlenses could be regularly and reversibly tuned through pH modulation. Owing to their tunable properties and complete biocompatibility, protein microlenses demonstrate significant potential in optical, electronic, and biomedical applications.

Close-packed MLA with high NA is suitable for high-resolution imaging[177,178]. Wu et al. successfully fabricated high-quality MLAs using an equal-arc scanning strategy[111] (Fig. 5c). The fill rate of the MLA was ~100%, and the NA was 0.46, which is much higher than the reported value of 0.13. The fabricated MLA exhibits high-resolution imaging capabilities. Hua et al. used FLA- and cavitation-assisted methods to prepare convex MLAs (Fig. 5d) with a fill factor of up to 100% on sapphire crystals, which is difficult to achieve using other techniques[71]. This technology allows the manufacture of MLAs of arbitrary sizes, curvatures, and surface types.

Schmid et al. described a novel and easy method for creating 3D-printed opaque structures using a highly absorptive photoresist. This technique can be employed for the production of microscopic apertures, contrast enhancement in 3D-printed microoptical elements, and realization of novel optical designs[179]. The hybrid design shown in Fig. 5e features a solitary IP-S lens and an IP-black diaphragm. The integration of black photoresists enables more complex optical designs and can effectively improve the imaging quality of optical elements.

Microoptical elements based on the principle of reflection

Compared with refractive microoptical elements, reflective microoptical elements have the advantage of inherent achromatic properties[180]. Three categories of reflective optical elements are processed using FsLDW. The first is an optical element processed using a femtosecond laser, which inherently exhibits a good reflective surface. Deng et al. used a single-pulse femtosecond laser wet etching (SP-FLWE) technique to fabricate large-area concave all-silicon MLAs[157] rapidly. This method can produce approximately three million microlenses with parabolic profiles within 1 h (Fig. 5f). In addition, because the microlens height and aperture exhibit

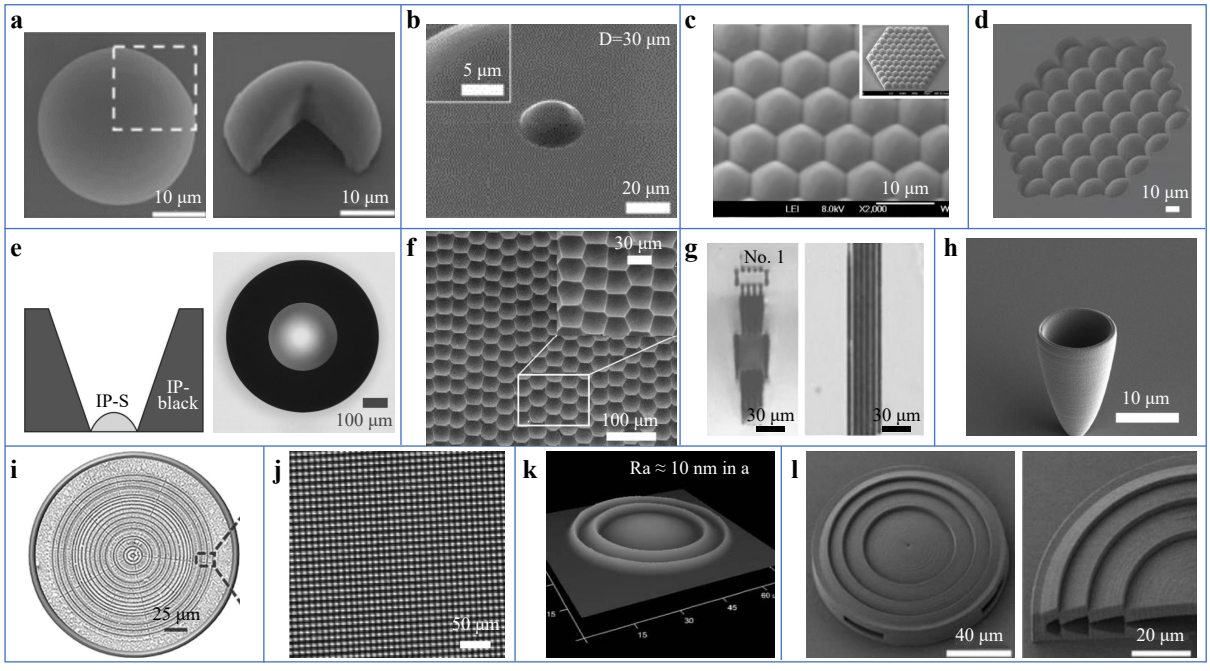

Fig. 5 a–e Refraction in the microoptical elements. **a** SEM image of concave–convex microlens (CCML) [obtained from ref. 176]. **b** Protein microlens [obtained from ref. 126]. **c** High-quality microlens arrays (MLA) with designable Nas [obtained from ref. 111]. **d** MLA with high numerical aperture (NA) [obtained from ref. 71]. **e** Prototype IP-Black aperture and lens made from IP-S [obtained from ref. 179]. **f–h** Reflection micro-optical elements. **f** Large-area concave all-silicon MLAs [obtained from ref. 157]. **g** Rectangular depressed-cladding waveguides written by the femtosecond laser in 6H –SiC crystals [obtained from ref. 182]. **h** 3D microphoton parabolic beam directors [obtained from ref. 183]. **i–l** Diffractive microoptical elements. **i** SEM image of the metalens [obtained from ref. 196]. **j** Custom volume gratings (grids) [obtained from ref. 192]. **k** Protein hydrogel-based continuous relief harmonic diffraction microlens [obtained from ref. 201]. **l** Multilayer diffraction structure [obtained from ref. 106].

an approximately proportional relationship with the laser scanning speed, MLA of different sizes can be easily obtained by varying the laser scanning speed. A reflective homogenizer MLA with a fill factor of 99% was tested using a He–Ne laser. The results reveal that the output beam through the MLA has a uniform light intensity distribution. Because of their transparency in the infrared region, these concave silicon MLAs can be extended to infrared light for homogenization.

The second type is the total internal reflection (TIR) optical element processed using the total reflection principle. Bianchi et al. prepared a microparabolic reflector using a photocured resin consisting of a diacrylate monomer[181]. The center of the structure was a sphere centered at the focal point of the paraboloid. Because of total internal reflection, the light propagating inside the outer fiber core was reflected by the lateral parabolic surface. In this structure, the reflected light was incident perpendicular to the sphere, minimizing the deflection owing to refraction. In addition to the large NA, parabolic reflectors can also focus independently of the submerged medium because they do not depend on refraction. A waveguide (lightguide) is a reflective microoptical element modulated by the refractive index that utilizes the principle of total internal reflection to guide light along a specific path efficiently. It demonstrates extensive applications in integrated optoelectronic devices. Various waveguide structures based on transparent materials have been prepared using the FsLDW technology, including single-, double-, vertical-dual-line, multiple-line, ridge, and depressed claddings. Zhang et al. prepared double-line and depressed-cladding waveguides in 6H-SiC (silicon carbide) crystals using the FLM (as shown in Fig. 5g)[182]. The mode distribution could be adjusted by changing the processing parameters of the waveguides. Their study provided a method for manufacturing low-loss waveguides in 6H-SiC crystals, which is important for future SiC-based integrated quantum photonics.

The last category involves the deposition of metals onto the surface of an element to form reflective optical elements. Atwater et al. used a femtosecond laser to produce 3D microphoton parabolic beam directiors[183] (Fig. 5h). After coating with 20 nm chromium and 380 nm silver using a plasma sputtering coater, the optical aperture

was etched to the bottom of the paraboloid using focused ion beam lithography. Finally, a set of micron-scale silver-coated 3D paraboloid structures was obtained and anchored to the silver-coated substrate at the bottom of the paraboloid. Microphoton parabolic light directors can be used to design the collimating beam of advanced solar cells and LED.

Microoptical elements based on the principle of diffraction

Diffractive microoptical elements (DOEs) are divided into harmonic diffractive optical elements (HDOE), single-layer diffractive optical elements (SLDOE), and multilayer diffractive optical elements (MLDOE)[184–187]. DOEs use the 3D relief structure of their surfaces to modulate and transform the wavefront phase and are characterized by lightness and thinness, design flexibility, free modulation of the incident light, and batch reproducibility[122]. Compared to conventional refractive and reflective optical elements, DOEs can simplify structures, reduce weight and volume, and improve the imaging quality of conventional optical systems[188,189].

Various SLDOEs have been successfully fabricated over the last few years[190]. Based on BSA and PDMS, Sun et al. fabricated a new soft diffractive microoptical element using the TPP technique, named microscale kinoform phase-type lens (micro-KPL)[191]. Even in strongly acidic or alkaline environments, micro KPL offers excellent surface quality, precise 3D shape, and unique optical properties. Using sol–gel materials and TPP technology, Hong's team prepared a single-sided diffraction grating with a linear shrinkage of 17% after heat treatment at 600 ℃[130,192]. The 3D printing of glass microoptical elements with isotropic shrinkage, micron resolution, low peak-to-valley deviation (<100 nm), and low surface roughness (<6 nm) can be achieved in this manner.

Lin et al. reported a method for converting 2D monolayer materials into ultrathin flat lenses using FLM[166]. Sufficient phase or amplitude modulation can be obtained by generating a localized scattering medium within a monolayer of material via the FLM. Efficient 3D focusing can be realized through subwavelength resolution and diffraction-limit imaging, which allows diffraction-limit imaging at different magnification rates at different focal locations. Ultrathin lenses with subwavelength thicknesses are promising alternatives to conventional refractive lenses and demonstrate potential applications in miniaturized and compact imaging systems[193–195]. Wei et al. used the FLA method to demonstrate a broadband zoom graphene metalens with a thickness of 250 nm, which covers the entire visible spectrum (Fig. 5i)[196]. The fabricated graphene metalens enabled continuous and simultaneous adjustment of the focal length of light with different wavelengths. Laterally stretching the lens, a focal adjustment range of >20% can be achieved for three wavelengths (650, 550, and 450 nm).[197,198]. Laser-modified hydrogel materials are used to produce volume and subsurface diffraction gratings[192]. Densification of the hydrogel was achieved by controlling the laser power, speed, and penetration depth, and relevant changes in the local refractive index (RI) were described. Variations in RI facilitated the processing of customized volume gratings (parallel lines, grids, squares, and ring gratings) in the hydrogel (Fig. 5j).

A conventional single-layer DOE can achieve 100% diffraction efficiency only at the designed wavelength. Because of the severe wavelength dependence, the diffraction efficiency decreases substantially with the deviation in the incident wavelength. The HDOE, proposed by Dean Faklis et al., is characterized by the requirement that the optical path length between adjacent surfaces be an integer multiple of the design wavelength λ_0[199]. HDOE can obtain the same focal length at a series of separated wavelengths, effectively eliminating imaging chromatic aberration, and is widely used in infrared imaging systems[200]. Sun et al. constructed a protein-based harmonic diffraction microlens (PHDM)[201], as shown in Fig. 5k. With the excellent 3D morphology provided by the TPP, the PHDM exhibits remarkable harmonic diffraction optical properties and good focusing and imaging performance. Because of the irritability of the protein molecule, the focal length of PHDM can be easily adjusted in a few seconds by changing the pH value (focal length tunability of up to ~20%), resulting in unique pH-responsive behavior and good biocompatibility.

Arieli et al. proposed the design of microstructures with different concave and convex shapes by matching and combining two diffraction elements with different dispersion coefficients, which is defined as MLDOE. Thus, aberrations can be eliminated in a broad spectrum depending on the different phases required for different combinations. Hu et al. fabricated an SU-8 microstructure with an arbitrary continuous surface and high precision using TPP[188], as shown in Fig. 5l[106]. The wideband operating characteristics of MLDOE can achieve an average diffraction efficiency of >84%, which is maintained above 80% over the entire visible band (406–824 nm). With the rapid development of integrated quantum photon technology, the design and preparation strategies for wideband MLDOEs have attracted considerable attention and are widely used.

Hybrid-principle microoptical element (HOE)

Compared with single diffractive optics, HOE exhibits unique dispersion, excellent thermal properties, monochromatic aberration correction capability, and wavefront correction capability, which can improve the design flexibility and overcome several limitations of conventional optical elements. HOE can be divided into hybrid refractive–diffractive optical elements (HRDOE) and hybrid refraction–reflection optical elements (HRROE). The HRDOE exhibits several advantages over conventional optical elements in improving image quality[188], reducing size and cost. Hua et al. designed and fabricated a hybrid diffractive refractive lens (HDRL) using FsLDW[202]. As shown in Fig. 6a, the diffractive section is an achromatic element with a diameter of 10 mm situated within a Z-cut sapphire substrate, whereas the refractive portion consists of a spherical plano-convex lens. HDRL exhibits superior imaging performance in terms of the modulation transfer function compared to a single spherical lens. Fabricating diffractive elements inside the spherical lens not only further improves the thermal stability of the optical system but also reduces its size and weight. Tian et al. proposed a small and simple optical vortex beam generator called a hybrid refractive–diffractive optical vortex microlens (HOVML)[203], as shown in Fig. 6b. A helical dislocation plate was integrated into a normal SU-8-based microlens using TPP. The HOVML generates optical vortex beams using only one refractive–diffractive hybrid microlens. The optical properties of the HOVML simulated in the far field agreed with the experimental results. Moreover, the theoretical conversion efficiency of the HOVML is higher than that of multienergy and amplitude-type diffractive elements owing to its continuous surface structure. Optical vortex beams have promising applications in various fields, such as optical communication, quantum information, and astronomy.

Multimaterial HRDOE exhibits more abundant functions than single-material elements, such as excellent achromatic properties. Timo et al. processed a hybrid material system using two different photoresists (Fig. 6c)[204]. They first used IP-Dip to fabricate chiral photonic crystal structures on the end faces of optical fibers as circularly polarized filters. The HRDOE was fabricated using the IP-S, which consisted of saddle-shaped free-form lenses with Fresnel zone plates (FZPs) on top. With photonic crystals and an HRDOE, the system is capable of both polarization control and beam shaping. Michael et al. processed optical elements with excellent achromatic properties using two materials (IP-S and IP-N162), as shown in Fig. 6d[121]. The apochromat includes a refractive aspherical portion and step portion of the diffractive surface. IP-N162 and IP-S were used to prepare the base and the top of the apochrome, respectively. The apochromatic/achromatic lens exhibits design flexibility and can be used at different wavelengths, such as 500, 600, and 700 nm. Li et al. investigated an HRROE suitable for high-NA side-viewing configurations to capture fluorescent emission light[205]. In the TIR lens, light undergoes TIR and is directed toward each of its 'teeth,' where it is refracted on the second surface (Fig. 6e). Leveraging the degrees of freedom associated with reflection and refraction within a confined space enables an exceptionally compact design.

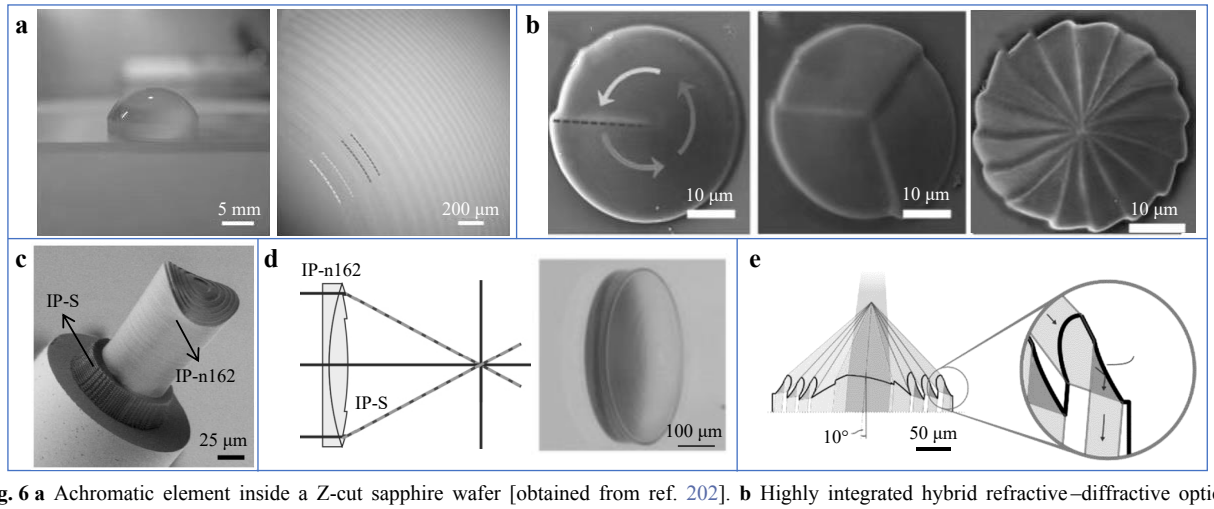

Fig. 6 a Achromatic element inside a Z-cut sapphire wafer [obtained from ref. 202]. **b** Highly integrated hybrid refractive–diffractive optical vortex microlens (HOVML) [obtained from ref. 203]. **c** Polarization control and beam shaping on a fiber [obtained from ref. 204]. **d** Achromatic lens is made of two materials [obtained from ref. 121]. **e** Hybrid refraction and total internal reflection lenses [obtained from ref. 205].

Stereoscopic systems

Stereoscopic systems are integrated systems formed by multiple optical elements combined in the horizontal or vertical direction and are widely used in optoelectronics[206], biomedicine[207–209], robotics, and microfluidics[210]. The optical elements in a stereo system are connected via auxiliary structures, all of which are processed using a femtosecond laser. This section focuses on the auxiliary structures and several typical imaging/nonimaging applications of stereoscopic systems. Imaging applications include integrated imaging systems, imaging systems combined with microfluidics, and imaging systems for optical storage. Nonimaging applications include optical modulation systems, spectral inspection systems, and waveguide-based photonic chip systems.

Auxiliary structure of stereoscopic systems

Processing auxiliary structures is necessary in addition to developing individual optical elements. For example, when processing a system with multiple elements, auxiliary structures are required to connect multiple optical elements (as shown in Figs. 7a–c). These auxiliary structures are processed directly during the fabrication of the optical elements. Thus, they can be used to precisely locate the distance between elements. To facilitate the combination of optical elements and fibers, an auxiliary structure called a fiber chuck was proposed by Parvathi (Fig. 7d)[211]. One end of the fiber chuck was integrated with optical elements, and the other end was designed as a structure that could be inserted using optical fibers. In addition, another structure in the chuck limits the insertion depth of the optical fiber, reducing manual alignment and distance errors. Auxiliary structures are also suitable for elements that undergo deformation during processing. For example, processing structures based on organic and inorganic hybrid glass materials along with the glass substrate must be heat-treated after TPP, during which the structure shrinks and deforms. Therefore, designing precompensated deformation structures is necessary. As shown in Fig. 7e, the precompensation structure between the optical element and glass substrate prevents distortion of the element. Fig. 7f shows the PDMS-based auxiliary structures with elastic deformation[191]. Protein optical elements processed on PDMS substrates demonstrate good elasticity and scalability. Auxiliary structures also help improve the imaging quality, such as apertures. Tan et al. designed and processed a simple double-sided microlens system using SU-8 (Fig. 7g)[212]. They plated an opaque metal film on one side of a glass substrate to form an aperture. By integrating the aperture as an auxiliary structure into the system, excess light can be prevented from entering the lens, effectively improving the imaging quality. Weber et al. produced an aperture in a 3D-printed micrography system using Ag shadow evaporation[51]. Commercially available rust solutions can oxidize Ag films to produce a low-reflectance layer that can serve as an excellent aperture. The combination of optical and auxiliary structures can expand the number of functions.

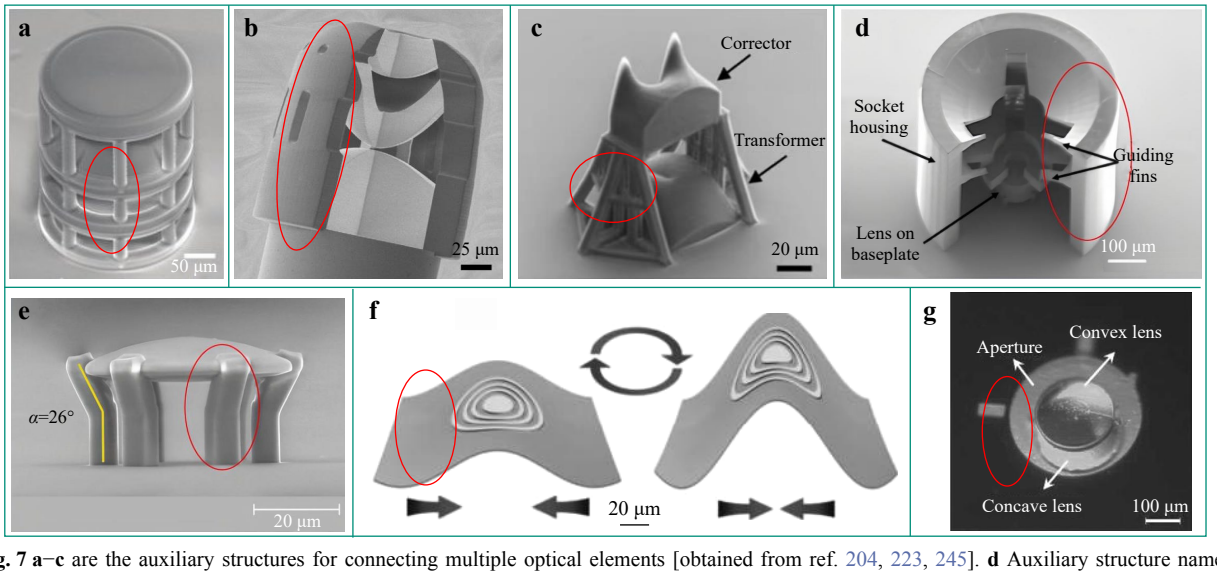

Fig. 7 a–c are the auxiliary structures for connecting multiple optical elements [obtained from ref. 204, 223, 245]. **d** Auxiliary structure named fiber chuck [obtained from ref. 211]. **e** Precompensated deformation structures [obtained from ref. 133]. **f** Flexible auxiliary structure [obtained from ref. 191]. **g** Aperture in the double-sided optical system [obtained from ref. 212].

Imaging stereoscopic system

Integrated imaging system

Optical imaging is the most common application for optical elements. Lens systems can be constructed by combining multiple lenses to achieve more complex imaging[213,214]. For example, for wide-angle and large field-of-view imaging, multiple lenses with aspherical shapes are necessary to obtain superior optical performance and correct the aberrations[215–217]. Thiele et al. proposed a stacked imaging system with multiple integrated optical elements[218]. The system was manufactured in one step by TPP without requiring alignment and assembly of minimal optical elements (<200 μm in diameter and <100 μm in height). The lens system enables submicron-resolution imaging at visible wavelengths and has a field-of-view of up to 60°. The field-dependent optical aberration can be compensated for by increasing the number of refractive interfaces in the lens system. Stacked-lens systems offer excellent optical performance and are compact, at least an order of magnitude smaller than other lens systems. Galvez et al. reported the performance of three closed-focus microendoscopic distal optical systems[219] (Fig. 8a). Each system used the same aperture stop placed in front of the distal optical element, and the same fiber bundle, proximal optical system, and camera. The distal optical systems they processed exceeded expectations for the working distance and angular field of view. Several microobjective lenses with different fields of view were printed on the surface of the fiber to achieve a perfect fusion of the optical fiber and objective lens.

Compound eyes (CE) is a natural multiaperture optical imaging system that shows significant potential in modern optics[220]. Hu et al. reported a bionic μ-CE camera with an integrated optoelectronic system (Fig. 8b)[17]. The contour of each processed eye was designed according to a logarithmic function, which can considerably increase the depth of field and focus range of small eyes. The obtained μ-CEs are integrated with a commercial complementary metal-oxide semiconductor (CMOS) detector to form a μ-CE camera, which enables large field-of-view (90°) imaging, spatial position recognition, and the trajectory monitoring of moving targets. In addition to processing optical elements directly on optical fibers, optical elements can be processed directly on the surfaces of light-emitting diodes and image sensors. Thiele et al. demonstrated a highly miniaturized camera[221] that could imitate the natural vision of predators by printing different multilens systems directly on CMOS image sensors[215]. As shown in Fig. 8c, four lens systems with different focal lengths were combined in a 2 × 2 arrangement to achieve a 70° field of view.

Li et al. used the TPP technique to process a miniaturized endoscope directly on an optical fiber, solving conflicting issues in the design of multimode microendoscopes[205], as demonstrated in Fig. 8d. This endoscope included an external lens for achieving high NA (0.8) fluorescence and an internal lens for achieving low NA (0.08) optical coherence tomography (OCT). The lens contains different but connected optical surfaces with a 330 μm diameter for fluorescence and OCT imaging. The microlens can achieve a sensitivity gain of more than 10 times, allowing for in vivo OCT and fluorescence at a lower laser power and fluorescent dye concentration, thus reducing the toxicity of the dye[222].

This light-guide system can be used for snapshot hyperspectral imaging. Liang et al. developed a compact high-resolution snapshot hyperspectral imaging (HSHI) system using photoconductive arrays fabricated from a sol–gel glass material (Fig. 8e)[223]. Optical devices project an object onto the center of the input plane within a processed light-guide array. By arranging the output side of the light-guide array, the spectrum from each light guide can be parsed into the sensor with minimal crosstalk after passing through the collimating element, dispersing optics, and focusing element. The input and output surfaces of the light guide array can be processed into different shapes, such as concave surfaces. Concave surfaces can significantly simplify optical systems by eliminating the need to correct field curvature, which is a major complicating factor in optical design. Therefore, HSHI systems exhibit exceptional compactness and high spatial resolutions.

Imaging system combined with microfluidics

In recent years, integrating imaging microoptical elements with microfluidic chips has attracted wide attention, showing significant potential for applications in optical capture, fluidic lasers, tunable optics, etc.[224–226]. Lu et al. used TPP to fabricate solvent-tunable PDMS microlenses[227]. PDMS microlenses exhibit exceptional optical properties attributed to their high-precision and smooth surfaces, as well as their unique solvent-tunable characteristics. The focal length can be changed using different concentrations of organic solvents[228]. Furthermore, because of the small size of the microlens, the relatively large boundary area promotes solvent diffusion, shortening the response time required for the expansion and contraction of the lens, which can be accomplished within a few seconds. This microoptical element can be flexibly integrated into a microfluidic device, which will provide new functions to common microfluidic chips, such as optical focusing, optical imaging, and in situ monitoring.

Fig. 8 a Close-focal microendoscopic on an optical fiber [obtained from ref. 219]. **b** Bionic Compound eyes (CE) camera with an integrated optoelectronic system [obtained from ref. 17]. **c** 3D-printing different multilens objectives directly onto a complementary metal-oxide semiconductor (CMOS) [obtained from ref. 215]. **d** Multimodal microendoscopic for fluorescence and optical coherence tomography (OCT) imaging [obtained from ref. 205]. **e** Lightguide system used for snapshot hyperspectral imaging [obtained from ref. 223].

Wu et al. integrated flexible 3D polymer micro-optical elements into the channels of microfluidic glass elements[229,230], as shown in Fig. 9a. They used wet etching-assisted laser ablation to process the channels inside the glass and SU-8 to process the optical elements (2D FZPs and 3D refraction MLAs) inside the channels. The optical elements in the channel feature multicolor focusing and an enlarged focal length (greater than three times) and are capable of imaging in liquid channels. Processed optofluidic chips can achieve a success rate of up to 90% for uncoupled white blood cell counting. They designed and fabricated an optical fluidic system with two MLAs and a W filter for advanced cell filtration and counting.

Based on hybrid 3D printing technology, Tan et al.

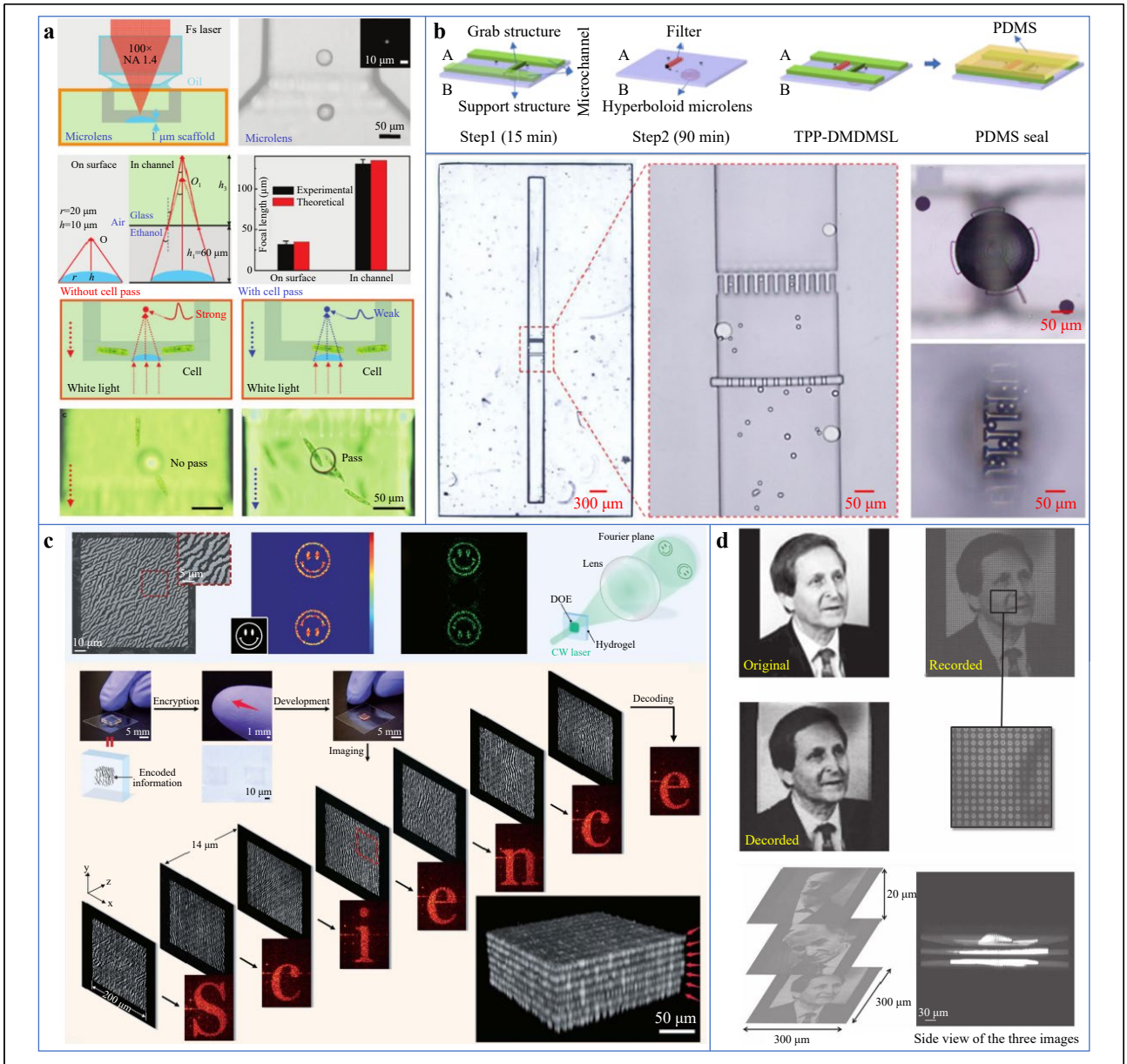

Fig. 9 a Optofluidic chip was used for uncoupled white light cell counting [obtained from ref. 229]. **b** Multifunctional double-sided microfluidic system [obtained from ref. 105]. **c** Fabrication of DOE and its applications in 3D optical storage and encryption. Fluorescent images of the decrypted holograms, in which "Science" is decoded [obtained from ref. 170]. **d** Pictures embedded in the glass were written with a NIR femtosecond laser and read with NUV light [obtained from ref. 231].

designed and processed a multifunctional double-sided microfluidic system using SU-8 and PDMS material[105]. Fig. 9b shows a schematic of the double-sided microfluidic system, which consists of a microchannel, filtering structure, collection structure, and hyperbolic imaging lens. The microchannels and filter structures were processed using a DMD lithography system, while the hyperbolic lens and collection structures were processed using TPP. After the channel was sealed, the particles flowed into the channel with the liquid, and particles of the required size were collected after passing through the filter and collection structure. Simultaneously, the hyperbolic lens on the other side of the substrate allowed real-time observation of the collection, enabling a multifunctional microfluidic system. Experimental tests showed that the double-sided microfluidic chip offers excellent performance for the filtration of multisized particles and real-time imaging of collected particles.

Imaging systems for optical storage

3D imaging systems constructed using femtosecond

laser processing can also be used for data storage applications[231–233]. By processing hydrogels using FLM, Han et al. demonstrated a method for optical storage and encryption of optically written information by physically shrinking 3D nanostructures (Fig. 9c)[170]. They fabricated a seven-layer structure that encodes the word 'Science,' with each layer containing a 200 × 200 pixel hologram. The designed holograms were patterned on a fully expanded gel using the FLM. After the complete acid-induced hydrogel shrinkage, each pixel was reduced to ~150 nm, resulting in a storage density of 20 Tb/cm^3. As the feature size of a 3D structure is below the diffraction limit, only translucent rectangles lacking structural details can be observed using an optical microscope. Therefore, the processed pattern is completely invisible, and the information stored in the structure is effectively encrypted. Moreover, the contracted and desiccated hydrogels are chemically stable and endure prolonged storage. The redevelopment of these structures in a 0.5 mM aqueous NaOH solution and deposition with fluorescent materials enable the decryption of stored holograms, which can be read out by confocal microscopy.

Huang et al. used femtosecond laser ablation to store information by writing 3D patterns of perovskite quantum dots (QDs) onto glass materials[234]. High luminescent CsPbBr3 QDs can be reversibly fabricated or decomposed in situ by FLM or thermal annealing (350 ℃), respectively. This writing and wiping pattern can be repeated for several cycles, and the luminescent QDs are well protected by the inorganic glass substrates. Zinc phosphate glass is a femto-photoluminescent glass containing silver ions. When excited by NUV radiation, no noticeable change is observed in the refractive index; however, it exhibits notable fluorescence and nonlinear optical properties. Royon et al. demonstrated the use of a zinc phosphate glass for 3D optical recordings (Fig. 9d)[231]. This method provides the advantages required for 3D optical data storage, such as high storage capacity (up to hundreds of TB/cm^3), high read speed (500 Mbit/s), no crosstalk, and no photobleaching of fluorescence. Furthermore, the temperature and aging tolerances of zinc phosphate glass have made it suitable for perennial storage for centuries.

Nonimaging stereoscopic system

Optical modulation system

Beam shaping generally refers to homogenizing an inhomogeneous beam (Gaussian beam, etc.) and forming it into a desired shape, such as a rectangle, hexagon, and circle[235–237]. Gissibl et al. fabricated phase masks directly on the end surfaces of single-mode fibers using TPP to achieve intensity shaping of the output beam[238]. Because the intensity-shaping phase mask was fabricated directly on the fiber core, the intensity distribution of the emitted light was highly symmetrical. Thiele et al. used IP-S to fabricate dielectric concentrators on LED chips, providing unprecedented collimation efficiency[239,240] (Fig. 10a). They tested LEDs at a forward current of 10 mA and recorded the illumination distribution before and after processing the dielectric concentrator. In the collimation direction, the output light intensity increased by 6.2 times when diameters and lengths were <200 μm, and the emission half-angle decreased by 50%. This method allows for arbitrary geometries within a very small range and is suitable for miniaturizing optical elements[241]. An integrated single-photon source with a high optical extraction efficiency is a critical structure for applications in quantum communication[242]. Fischbach et al. achieved a single-photon source with excellent quantum optical properties and high extraction efficiency by directly processing a microobjective lens on a QD microlens[243]. Compared with structures without a microobjective, the photon-extraction efficiency improved 2.3 times. Meanwhile, excellent single-photon purity was maintained, and the required excitation power was reduced by an order of magnitude. Further optimization of the microlens/microobjective device will significantly enhance its potential as a highly efficient method for achieving fiber-coupled single-photon sources.

Optical tweezers are formed when the optical field is modulated by an optical vortex, which can be used for particle capture[244]. Shlomi et al. fabricated a miniature vortex mode sorter that enabled direct integration of the sorter into an optical system[245]. They proposed a sorter comprising two independent elements and an integrated device. These elements can handle pure vortex beams and mixed vortex beams with topological charges of $|L| \leqslant 3$ and $|L| \leqslant 2$, respectively. The integrated sorters were fabricated via a continuous printing process using IP-Dip. Importantly, the integrated sorter cannot be processed using other methods, such as diamond turning or computer numerical control milling.

Yu et al. demonstrated a new type of on-chip optical tweezer, which is a free-form microoptical element based on waveguide integration[246]. As shown in Fig. 10b, this design enables the precise positioning of the trap in the 3D region above the chip and easy adjustment of the capture potential energy. In addition, microoptical elements can be seamlessly integrated with on-chip waveguides. This allows the elements to easily access a photonic integrated circuit to endow them with new functions, such as dynamic adjustment and switching of optical traps. Furthermore, freeform reflection or refraction microoptic elements offer excellent optical efficiency (>95% efficiency from the

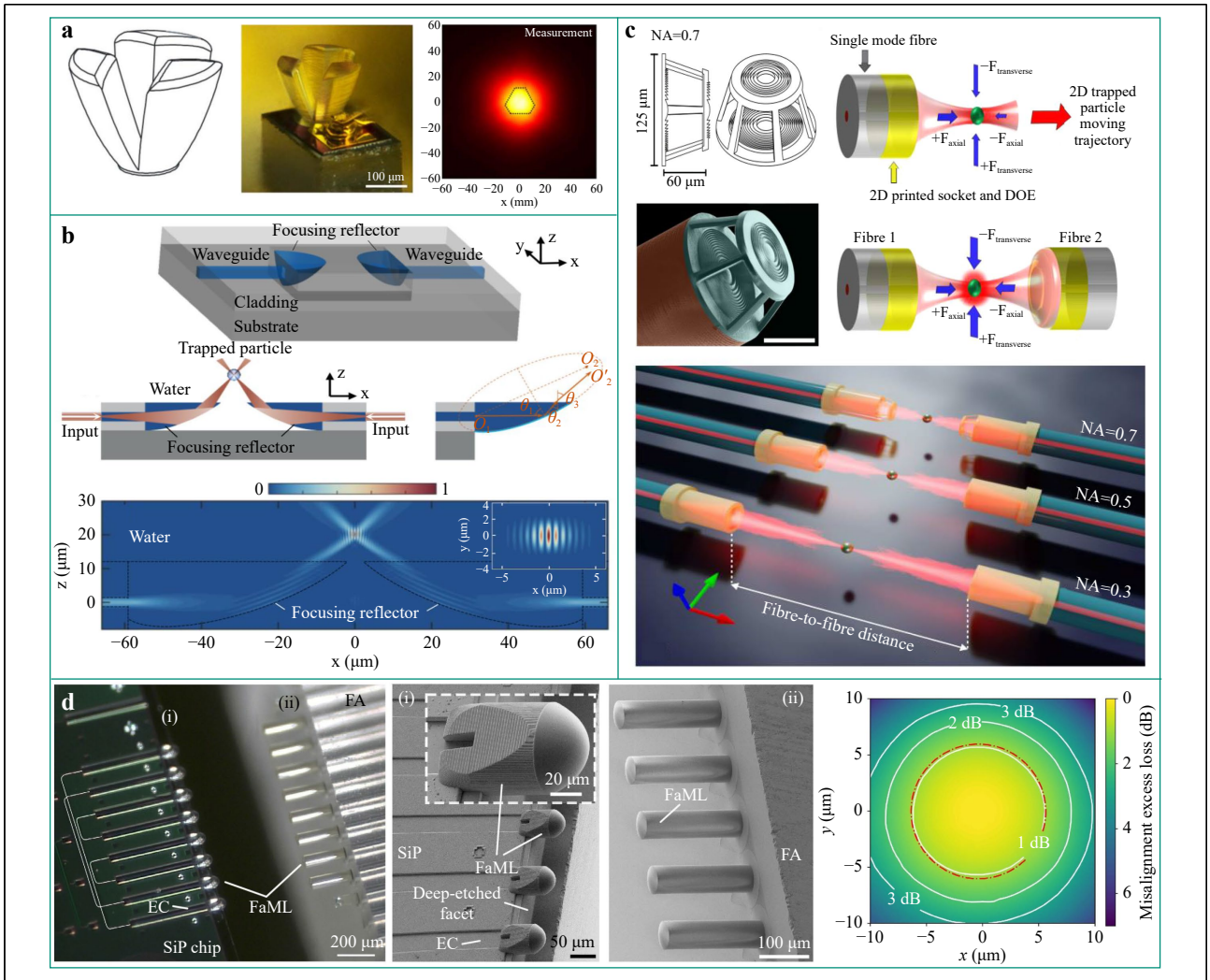

Fig. 10 a Dielectric concentrator on LED chips [obtained from ref. 239]. **b** On-chip optical tweezers [obtained from ref. 246]. **c** Efficient optical trapping technique based on reverse transmission fiber [obtained from ref. 247]. **d** Printing of microlenses on the surface of photonic chips and fibers to collimate and redirect beams. [obtained from ref. 248].

waveguide to the focus spot) and broadband operation. A high efficiency is beneficial for reducing the capture threshold power, whereas a large spectral bandwidth facilitates the preparation of quantum states and fluorescence excitation. Finally, the real-time motion of the captured particles can be monitored by measuring the intensity of the scattered light.

Asa et al. proposed an efficient optical trapping technique based on a reverse transmission fiber that uses a converged fiber with a 3D-printed diffractive Fresnel lens on its surface[247]. Based on the basic principle of conventional optical trapping, increasing the NA of the focused beam changes the distribution of optical forces, leading to optical trapping in both the lateral and axial directions, as shown in Fig. 10c. Therefore, superimposition of two identical 2D trapping spots can generate a focal region. They fabricated three different Fresnel lenses on the fiber surface, which showed very stable trapping ability for dielectric particles in water. Xu et al. used TPP to fabricate microlenses to assemble advanced photonic systems[248]. They printed microlenses on the surfaces of photonic chips and fibers, allowing the beam to be shaped by the refractive plane, thus relaxing the axial and lateral alignment tolerances (Fig. 10d). Particularly, the emitted beam can be aligned to relatively large diameters independent of the device-specific mode field. This avoids using expensive active alignment methods and allows discrete optical elements to be placed in the free-space beam path between the photonic integrated circuits. They demonstrated the feasibility and versatility of the method through a series of demonstrations, which is an attractive path for the

assembly of advanced photonic systems.

Spectral inspection system

Various miniaturized spectrometer concepts have been demonstrated and widely used. Spectrometers are divided into three main categories: direct, computational, and filtering methods. Direct spectrometers processed by Toulouse using the TPP occupied at least two orders of magnitude less space than spectrometers processed using other methods[249]. Moreover, the spectral bandwidth per resolution of a direct spectrometer can be increased by one to three orders of magnitude. They theoretically evaluated the feasibility of the spectrometer in a miniature volume of $100 \times 100 \times 300\ \mu m^3$ and demonstrated it experimentally (Fig. 11a). The resolution of the fabricated spectrometer was 9.2 ± 1.1 nm at 532 nm and 17.8 ± 1.7 nm at 633 nm. This is the first spectrometer to demonstrate a direct spatial-spectral response in this range. Hong et al. demonstrated a compact spectral imaging system using TPP[250]. The microspectrometer layout with dispersion elements is illustrated in Fig. 11b, comprising a lens equipped with both a grating and a dispersive prism. The dispersive spectral distribution has been accurately captured by the CMOS camera. Overall, the femtosecond laser processing microspectrometer marks an innovation in the 3D printing of microoptics.

Waveguide-based photonic chip system

Today, various physical systems aimed at general-purpose quantum computing are moving toward increasing the number of controllable qubits and enabling large-scale quantum computations. Photons have several unique advantages, such as fast traveling speed, simple single-qubit operation, long coherence time, and multiple degrees of freedom, and are suitable for quantum computing[251]. Zhang et al. realized the non-Abelian weaving of multiple

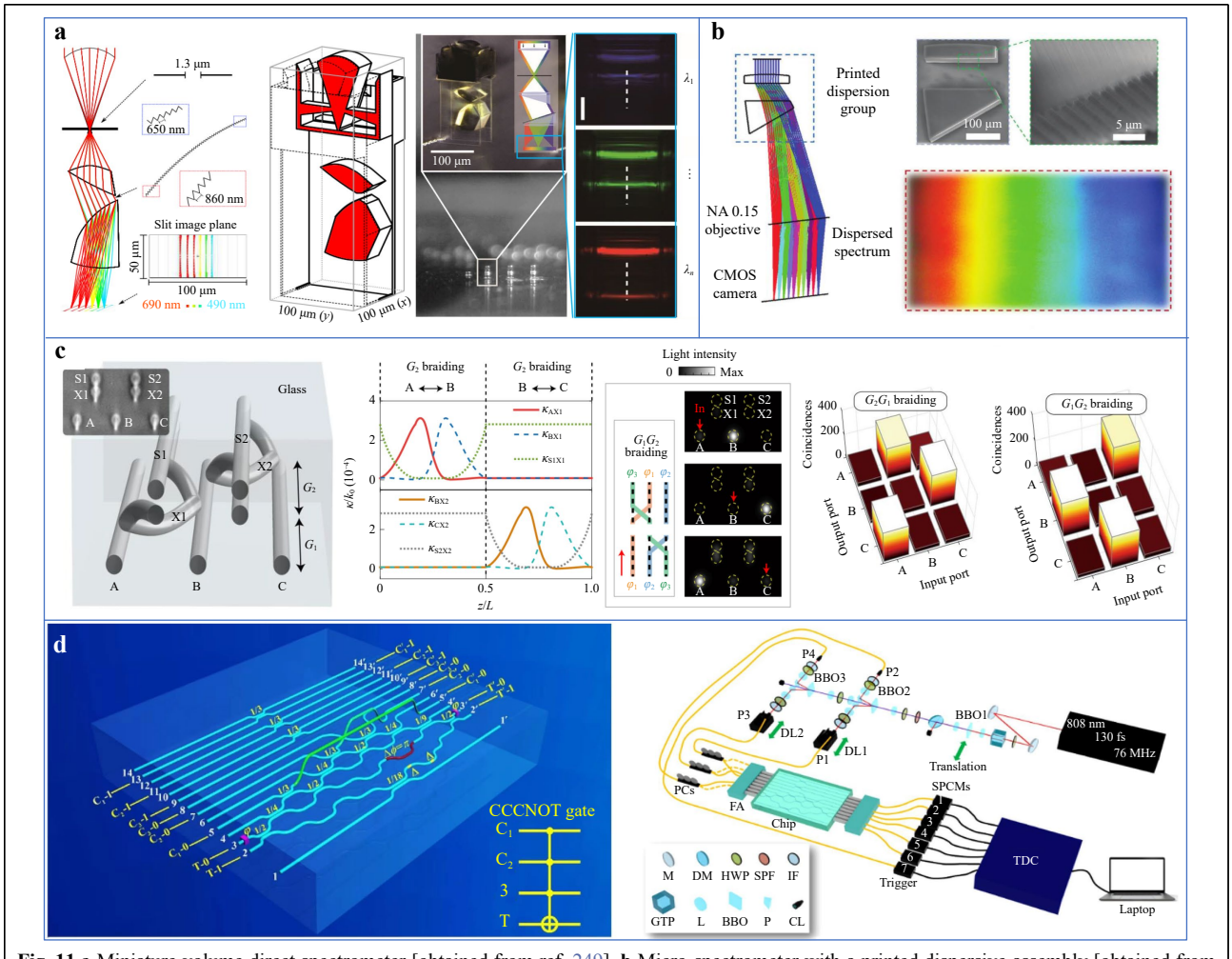

Fig. 11 a Miniature volume direct spectrometer [obtained from ref. 249]. **b** Micro-spectrometer with a printed dispersive assembly [obtained from ref. 250]. **c** Non-abelian weaving of multiple photon modes on a photon chip [obtained from ref. 252]. **d** On-chip path-encoded photonic quantum Toffoli gates [obtained from ref. 253].

photon modes on a photon chip[252]. As shown in Fig. 11c, chiral symmetry was used to ensure the degeneracy of multiple zero modes and drive them in a synchronous adiabatic evolution, thereby generating a unitary geometric phase matrix for the exchange of photon residence positions. Researchers have observed up to five modes of on-chip non-abelian weaving using both classical light and single photons. Quantum logic gates are used to construct quantum circuits in general-purpose quantum computers. Using optimized 3D structures with overpass waveguides to reduce circuit complexity, Li demonstrated on-chip path-encoded photonic quantum Toffoli gates via FLM (Fig. 11d)[253]. In addition, they performed path encoding of a four-quantum-controlled NOT gate to confirm the scalability of this resource-saving technique.

Summary and Outlook

FsLDW demonstrates the ability of true 3D processing to integrate the molding of complex 3D structures and meet the processing accuracy requirements of microoptical components. Therefore, it is a crucial technology for preparing three-dimensional integrated optical systems. This paper reviews the recent developments in FsLDW-enabled imaging/nonimaging optical elements, including processing methods, processable materials, different types of optical elements, and stereoscopic systems. Various optical elements and systems based on FsLDW have been developed, enabling various cutting-edge applications. Nevertheless, FsLDW remains a novel technology, and several important development directions can be speculated.

First, the femtosecond laser processing of stereoscopic systems requires various selectable materials. Polymer resin materials have been widely processed but are commonly hindered by issues such as toxicity and poor robustness. As an alternative, glass materials with high permeability, a broad spectrum, and superior mechanical strength are highly promising for the preparation of microoptical elements[254–256]. Currently, the sintering temperature of the organic–inorganic hybrid liquid glass material has decreased to 650 °C, enabling the integration of optical elements with specific devices that withstand high treatment temperature[257]. In addition to the continuously decreasing heat-treatment temperature, various liquid glass materials are becoming more abundant, resulting in more functions. For example, the refractive index of a liquid glass can be adjusted by adding different types of nanoparticles. Glass-ceramic materials have excellent optical properties, such as high transparency, low dispersion, and a high refractive index, and can be applied to optical systems through femtosecond laser processing with further development[141]. Unlike single-material optical systems, multimaterial optical systems consist of optical elements fabricated using different types of materials. The combination of different materials provides advantages such as a larger refractive index range, lower dispersion, and high nonlinear effects[258]. In the future, femtosecond lasers are expected to process multiple materials in one system to achieve more complex functions such as a negative refractive index and metalenses.

Second, stereoscopic systems processed by FsLDW usually contain multiple optical elements and couplers connecting the optical elements, significantly increasing the processing complexity and time[259,260]. Therefore, the development of efficient femtosecond laser processing methods is another important development direction[261–263]. For example, the HVLS method can improve processing efficiency by using small voxels to process the surface of optical elements and large voxels to process the auxiliary structures between optical elements and structures inside the optical elements.

Therefore, the development of multimaterial and efficient femtosecond laser processing methods will further promote the establishment of multisystem, multidimensional, multiscale, and multifunctional stereo optical systems (Fig. 12). For example, microoptical elements can be directly processed on a fiber to form a stereoscopic integrated system to achieve functionalities such as microimaging and spectral analysis. Traditional lenses usually require a certain thickness to achieve the lens effect, whereas metalenses can achieve super-resolution imaging, ultrathin focusing, reflection elimination, super zoom, and other functions by relying on their nanoscale or submicron structures, thus forming a planar optical system with excellent performance. Moreover, photonic chips with various functions can be constructed by combining and connecting waveguides with different optical elements or detectors, such as bionic

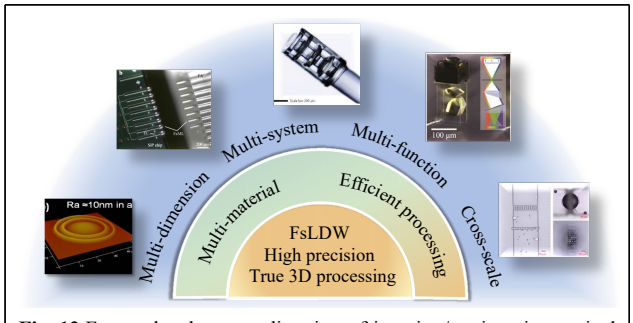

Fig. 12 Future development direction of imaging/nonimaging optical elements processed by FsLDW [obtained from ref. 105, 201, 219, 248, 249].

vision perception and optical communication modulator[248,264,265]. In general, to achieve various imaging/nonimaging functions in the extremely small spaces of miniaturized devices in the future, microoptical elements will continue to develop toward the direction of stereoscopic integration[266]. Further optimization and improvement of FsLDW technologies for the development of multimaterial, cross-scale, multidimensional, multiple systems, and multifunctional optical elements and systems are essential for practical and industrial applications.

Acknowledgements

This work was supported by the National Natural Science Foundation of China (Nos. 62275044, 62205174, 61875036), the Jinan "20 New Colleges and Universities" Innovation Team Introduction Project (202228047).

Author details

[1]Center for Advanced Optoelectronic Functional Materials Research, and Key Laboratory for UV-Emitting Materials and Technology of Ministry of Education, National Demonstration Center for Experimental Physics Education, Northeast Normal University, 5268 Renmin Street, Changchun 130024, China. [2]Wyant College of Optical Sciences, The University of Arizona, 1630 E. University Blvd, Tucson, Arizona 85721, USA. [3]Key Laboratory on Integrated Optoelectronics, College of Electronic Science and Engineering, Jilin University, Changchun 130012, China

Conflict of interest

The authors declare that they have no known competing financial interests or personal relationships that could have appeared to influence the work reported in this paper.

Received: 08 June 2023 Revised: 26 October 2023 Accepted: 30 October 2023
Accepted article preview online: 31 October 2023
Published online: 17 December 2023

References

1. Shin, D. et al. Scalable variable-index elasto-optic metamaterials for macroscopic optical components and devices. *Nature Communications* **8**, 16090 (2017).
2. Ohmori, H. et al. Ultraprecision micro-grinding of germanium immersion grating element for mid-infrared super dispersion spectrograph. *CIRP Annals* **50**, 221-224 (2001).
3. Yang, L. J. & Xing, T. W. Selection of the compensation quantity to the lens deformation caused by gravity. Proceedings of SPIE 9281, 7th International Symposium on Advanced Optical Manufacturing and Testing Technologies: Advanced Optical Manufacturing Technologies. Harbin, China: SPIE, 2014.
4. Yin, S. H. et al. Review of small aspheric glass lens molding technologies. *Frontiers of Mechanical Engineering* **12**, 66-76 (2017).
5. Chen, F. J. et al. Form error compensation in single-point inclined axis nanogrinding for small aspheric insert. *The International Journal of Advanced Manufacturing Technology* **65**, 433-441 (2013).
6. Chen, F. J. et al. Fabrication of small aspheric moulds using single point inclined axis grinding. *Precision Engineering* **39**, 107-115 (2015).
7. Jing, X. et al. Transverse additive manufacturing and optical evaluation of miniature thin lenses in ultracompact micro multi-spherical compound eye. *Optics and Lasers in Engineering* **151**, 106913 (2022).
8. Szkudlarek, K. et al. Terahertz 3D printed diffractive lens matrices for field-effect transistor detector focal plane arrays. *Optics Express* **24**, 20119-20131 (2016).
9. Zhang, H. et al. Rapid trapping and tagging of microparticles in controlled flow by *in situ* digital projection lithography. *Lab on a Chip* **22**, 1951-1961 (2022).
10. Behroodi, E., Latifi, H. & Najafi, F. A compact LED-based projection microstereolithography for producing 3D microstructures. *Scientific Reports* **9**, 19692 (2019).
11. Wang, Z. et al. Digital micro-mirror device -based light curing technology and its biological applications. *Optics & Laser Technology* **143**, 107344 (2021).
12. Jiang, M. L. et al. 3D high precision laser printing of a flat nanofocalizer for subwavelength light spot array. *Optics Letters* **46**, 356-359 (2021).
13. Malinauskas, M. et al. 3D microoptical elements formed in a photostructurable germanium silicate by direct laser writing. *Optics and Lasers in Engineering* **50**, 1785-1788 (2012).
14. Zhuang, H. Q. et al. Assessment of spinal tumor treatment using implanted 3D-printed vertebral bodies with robotic stereotactic radiotherapy. *The Innovation* **1**, 100040 (2020).
15. Furlan, W. D. et al. 3D printed diffractive terahertz lenses. *Optics Letters* **41**, 1748-1751 (2016).
16. Cai, S. X. et al. Microlenses arrays: fabrication, materials, and applications. *Microscopy Research and Technique* **84**, 2784-2806 (2021).
17. Hu, Z. Y. et al. Miniature optoelectronic compound eye camera. *Nature Communications* **13**, 5634 (2022).
18. Camposeo, A. et al. Additive manufacturing: applications and directions in photonics and optoelectronics. *Advanced Optical Materials* **7**, 1800419 (2019).
19. Chaudhary, R. P. et al. Additive manufacturing of polymer-derived ceramics: materials, technologies, properties and potential applications. *Progress in Materials Science* **128**, 100969 (2022).
20. Salter, P. S. & Booth, M. J. Adaptive optics in laser processing. *Light:Science & Applications* **8**, 110 (2019).
21. Liu, Y. Q. et al. Breakthroughs in projection-enabled additive manufacturing: From novel strategies to cutting-edge applications. *The Innovation* **4**, 100395 (2023).
22. Xue, D., Wang, Y. C. & Mei, D. Q. Multi-step exposure method for improving structure flatness in digital light processing-based printing. *Journal of Manufacturing Processes* **39**, 106-113 (2019).
23. Kang, M. S., Jin, H. & Jeon, H. Photonic crystal L3 cavity laser fabricated using maskless digital photolithography. *Nanophotonics* **11**, 2283-2291 (2022).
24. Yang, D. F. et al. Structural optimization and performance testing of gold microarray electrode fabricated by DMD lithography and electrodeposition. *Chinese Optics* **15**, 592-607 (2022).
25. Zhang, H. et al. Transparent and robust superhydrophobic structure on silica glass processed with microstereolithography printing. *ACS Applied Materials & Interfaces* **15**, 38132-38142 (2023).
26. Hou, Z. Z. et al. Direct ink writing of materials for electronics-related applications: a mini review. *Frontiers in Materials* **8**, 647229 (2021).
27. Ge, Q. et al. Projection micro stereolithography based 3D printing and its applications. *International Journal of Extreme Manufacturing* **2**, 022004 (2020).
28. Lichade, K. M., Joyee, E. B. & Pan, Y. Y. Gradient light video projection-based stereolithography for continuous production of solid objects. *Journal of Manufacturing Processes* **65**, 20-29 (2021).
29. Heinrich, A. et al. Additive manufacturing of optical components. *Advanced Optical Technologies* **5**, 293-301 (2016).
30. Zhang, Z. M., Meng, Q. W. & Luo, N. N. A DMD based UV lithography method with improved dynamical modulation range for the fabrication of curved microstructures. *AIP Advances* **11**, 045008

(2021).
31. Alam, F. et al. Prospects for additive manufacturing in contact lens devices. *Advanced Engineering Materials* **23**, 2000941 (2021).
32. Vaidya, N. & Solgaard, O. 3D printed optics with nanometer scale surface roughness. *Microsystems & Nanoengineering* **4**, 18 (2018).
33. Zolfaghari, A., Chen, T. T. & Yi, A. Y. Additive manufacturing of precision optics at micro and nanoscale. *International Journal of Extreme Manufacturing* **1**, 012005 (2019).
34. Chen, X. F. et al. High-speed 3D printing of millimeter-size customized aspheric imaging lenses with Sub 7 nm surface roughness. *Advanced Materials* **30**, 1705683 (2018).
35. Kuo, H. F. & Huang, Y. J. Resolution enhancement using pulse width modulation in digital micromirror device-based point-array scanning pattern exposure. *Optics and Lasers in Engineering* **79**, 55-60 (2016).
36. Chaudhary, R. et al. Additive manufacturing by digital light processing: a review. *Progress in Additive Manufacturing* **8**, 331-351 (2023).
37. Liu, C. et al. Correction of a digital micromirror device lithography system for fabrication of a pixelated liquid crystal micropolarizer array. *Optics Express* **30**, 12014-12025 (2022).
38. Yuan, C. et al. Ultrafast three-dimensional printing of optically smooth microlens arrays by oscillation-assisted digital light processing. *ACS Applied Materials & Interfaces* **11**, 40662-40668 (2019).
39. Kafle, A. et al. 3D/4D printing of polymers: fused deposition modelling (FDM), selective laser sintering (SLS), and stereolithography (SLA). *Polymers* **13**, 3101 (2021).
40. Manapat, J. Z. et al. 3D printing of polymer nanocomposites via stereolithography. *Macromolecular Materials and Engineering* **302**, 1600553 (2017).
41. Sun, C. et al. Projection micro-stereolithography using digital micro-mirror dynamic mask. *Sensors and Actuators A:Physical* **121**, 113-120 (2005).
42. Shao, G. B. , Hai, R. H. & Sun, C. 3D printing customized optical lens in minutes. *Advanced Optical Materials* **8**, 1901646 (2020).
43. He, Z. Q. et al. Adaptive liquid crystal microlens array enabled by two-photon polymerization. *Optics Express* **26**, 21184-21193 (2018).
44. Sugioka, K. & Cheng, Y. Ultrafast lasers—reliable tools for advanced materials processing. *Light:Science & Applications* **3**, e149 (2014).
45. Sygletou, M. et al. Advanced photonic processes for photovoltaic and energy storage systems. *Advanced Materials* **29**, 1700335 (2017).
46. Pingali, R. & Saha, S. K. Reaction-diffusion modeling of photopolymerization during femtosecond projection two-photon lithography. *Journal of Manufacturing Science and Engineering* **144**, 021011 (2022).
47. Toulouse, A. et al. High resolution femtosecond direct laser writing with wrapped lens. *Optical Materials Express* **12**, 3801-3809 (2022).
48. Eschenbaum, C. et al. Hybrid lithography: combining UV-exposure and two photon direct laser writing. *Optics Express* **21**, 29921-29926 (2013).
49. Saha, S. K. et al. Scalable submicrometer additive manufacturing. *Science* **366**, 105-109 (2019).
50. Zhang, Y. L. et al. Designable 3D nanofabrication by femtosecond laser direct writing. *Nano Today* **5**, 435-448 (2010).
51. Weber, K. et al. Distortion-free multi-element Hypergon wide-angle micro-objective obtained by femtosecond 3D printing. *Optics Letters* **45**, 2784-2787 (2020).
52. Cardenas-Benitez, B. et al. Pyrolysis-induced shrinking of three-dimensional structures fabricated by two-photon polymerization: experiment and theoretical model. *Microsystems & Nanoengineering* **5**, 38 (2019).
53. Khorasaninejad, M. et al. Metalenses at visible wavelengths: diffraction-limited focusing and subwavelength resolution imaging. *Science* **352**, 1190-1194 (2016).
54. Somers, P. et al. Rapid, continuous projection multi-photon 3D printing enabled by spatiotemporal focusing of femtosecond pulses. *Light:Science & Applications* **10**, 199 (2021).
55. Malinauskas, M. et al. Ultrafast laser nanostructuring of photopolymers: a decade of advances. *Physics Reports* **533**, 1-31 (2013).
56. Zhu, Y. Z. et al. Recent advancements and applications in 3D printing of functional optics. *Additive Manufacturing* **52**, 102682 (2022).
57. Gonzalez-Hernandez, D. et al. Micro-optics 3D printed via multi-photon laser lithography. *Advanced Optical Materials* **11**, 2370001 (2023).
58. Maruo, S., Nakamura, O. & Kawata, S. Three-dimensional microfabrication with two-photon-absorbed photopolymerization. *Optics Letters* **22**, 132-134 (1997).
59. Chung, T. T. et al. Design and two-photon polymerization of complex functional micro-objects for Lab-on-a-Chip: rotating micro-valves. *Journal of Neuroscience and Neuroengineering* **2**, 48-52 (2013).
60. Glezer, E. N. & Mazur, E. Ultrafast-laser driven micro-explosions in transparent materials. *Applied Physics Letters* **71**, 882-884 (1997).
61. Mochizuki, H. et al. Density characterization of femtosecond laser modification in polymers. *Applied Physics Letters* **92**, 091120 (2008).
62. Hildebrand, G. et al. Process development for additive manufacturing of alumina toughened zirconia for 3D structures by means of two-photon absorption technique. *Ceramics* **4**, 224-239 (2021).
63. Harinarayana, V. & Shin, Y. C. Two-photon lithography for three-dimensional fabrication in micro/nanoscale regime: a comprehensive review. *Optics & Laser Technology* **142**, 107180 (2021).
64. Fritzler, K. B. & Prinz, V. Y. 3D printing methods for micro- and nanostructures. *Physics-Uspekhi* **62**, 54-69 (2019).
65. Nocentini, S. *et al*. 3D printed photoresponsive materials for photonics. *Advanced Optical Materials* **7**, 1900156 (2019).
66. LaFratta, C. N. & Baldacchini, T. Two-photon polymerization metrology: characterization methods of mechanisms and microstructures. *Micromachines* **8**, 101 (2017).
67. Xing, J. F., Zheng, M. L. & Duan, X. M. Two-photon polymerization microfabrication of hydrogels: an advanced 3D printing technology for tissue engineering and drug delivery. *Chemical Society Reviews* **44**, 5031-5039 (2015).
68. Heidrich, S. et al. Optics manufacturing by laser radiation. *Optics and Lasers in Engineering* **59**, 34-40 (2014).
69. Liu, X. Q. et al. Rapid engraving of artificial compound eyes from curved sapphire substrate. *Advanced Functional Materials* **29**, 1900037 (2019).
70. Hua, J. G. et al. Fast fabrication of optical vortex generators by femtosecond laser ablation. *Applied Surface Science* **475**, 660-665 (2019).
71. Hua, J. G. et al. Free-form micro-optics out of crystals: femtosecond laser 3D sculpturing. *Advanced Functional Materials* **32**, 2200255 (2022).
72. Qiu, J. F. et al. Fabrication of high fill factor cylindrical microlens array with isolated thermal reflow. *Applied Optics* **57**, 7296-7302 (2018).
73. Huang, S. Z. et al. Fabrication of high quality aspheric microlens array by dose-modulated lithography and surface thermal reflow. *Optics & Laser Technology* **100**, 298-303 (2018).
74. Grigaliūnas, V. et al. Microlens fabrication by 3D electron beam lithography combined with thermal reflow technique. *Microelectronic Engineering* **164**, 23-29 (2016).
75. Liu, X. Q. et al. Etching-assisted femtosecond laser modification of hard materials. *Opto-Electronic Advances* **2**, 190021 (2019).
76. Liu, X. Q. et al. Optical nanofabrication of concave microlens arrays. *Laser & Photonics Reviews* **13**, 1800272 (2019).
77. Lian, Z. J. et al. Rapid fabrication of semiellipsoid microlens using thermal reflow with two different photoresists. *Microelectronic Engineering* **115**, 46-50 (2014).

78. Hua, J. G. et al. Laser-induced cavitation-assisted true 3D nano-sculpturing of hard materials. *Small* **19**, 2207968 (2023).
79. Wang, B. X. et al. Rapid fabrication of smooth micro-optical components on glass by etching-assisted femtosecond laser modification. *Materials* **15**, 678 (2022).
80. Skora, J. L. et al. High-fidelity glass micro-axicons fabricated by laser-assisted wet etching. *Optics Express* **30**, 3749-3759 (2022).
81. Yong, J. L. et al. A review of femtosecond-laser-induced underwater superoleophobic surfaces. *Advanced Materials Interfaces* **5**, 1701370 (2018).
82. Wang, Q. et al. Reconfigurable phase-change photomask for grayscale photolithography. *Applied Physics Letters* **110**, 201110 (2017).
83. Sundaram, S. K. & Mazur, E. Inducing and probing non-thermal transitions in semiconductors using femtosecond laser pulses. *Nature Materials* **1**, 217-224 (2002).
84. Wang, Q. et al. Optically reconfigurable metasurfaces and photonic devices based on phase change materials. *Nature Photonics* **10**, 60-65 (2016).
85. Wu, R. B. et al. Long low-loss-litium niobate on insulator waveguides with sub-nanometer surface roughness. *Nanomaterials* **8**, 910 (2018).
86. Li, L. Q., Kong, W. J. & Chen, F. Femtosecond laser-inscribed optical waveguides in dielectric crystals: a concise review and recent advances. *Advanced Photonics* **4**, 024002 (2022).
87. Hua, J. G. et al. Characterization of refractive index change induced by femtosecond laser in lithium niobate. *Journal of Laser Micro/Nanoengineering* **12**, 207-211 (2017).
88. Wei, D. Z. et al. Experimental demonstration of a three-dimensional lithium niobate nonlinear photonic crystal. *Nature Photonics* **12**, 596-600 (2018).
89. Xiong, Z., Kunwar, P. & Soman, P. Hydrogel-based diffractive optical elements (hDOEs) using rapid digital photopatterning. *Advanced Optical Materials* **9**, 2001217 (2021).
90. Bückmann, T. et al. Tailored 3D mechanical metamaterials made by dip-in direct-laser-writing optical lithography. *Advanced Materials* **24**, 2710-2714 (2012).
91. Wu, D. et al. Bioinspired fabrication of high-quality 3D artificial compound eyes by voxel-modulation femtosecond laser writing for distortion-free wide-field-of-view imaging. *Advanced Optical Materials* **2**, 751-758 (2014).
92. Rodríguez, S. Redefining microfabrication of high-precision optics. *PhotonicsViews* **17**, 36-39 (2020).
93. Aderneuer, T., Fernández, O. & Ferrini, R. Two-photon grayscale lithography for free-form micro-optical arrays. *Optics Express* **29**, 39511-39520 (2021).
94. Geng, Q. et al. Ultrafast multi-focus 3-D nano-fabrication based on two-photon polymerization. *Nature Communications* **10**, 2179 (2019).
95. Matsuo, S., Juodkazis, S. & Misawa, H. Femtosecond laser microfabrication of periodic structures using a microlens array. *Applied Physics A* **80**, 683-685 (2005).
96. Maibohm, C. et al. Multi-beam two-photon polymerization for fast large area 3D periodic structure fabrication for bioapplications. *Scientific Reports* **10**, 8740 (2020).
97. Kato, J. I. et al. Multiple-spot parallel processing for laser micronanofabrication. *Applied Physics Letters* **86**, 044102 (2005).
98. Yang, L. et al. Two-photon polymerization of microstructures by a non-diffraction multifoci pattern generated from a superposed Bessel beam. *Optics Letters* **42**, 743-746 (2017).
99. Yang, L. et al. Parallel direct laser writing of micro-optical and photonic structures using spatial light modulator. *Optics and Lasers in Engineering* **70**, 26-32 (2015).
100. Xu, B. et al. Hybrid femtosecond laser fabrication of a size-tunable microtrap chip with a high-trapping retention rate. *Optics Letters* **45**, 1071-1074 (2020).
101. Wang, Z. P. et al. High efficiency and scalable fabrication of fresnel zone plates using holographic femtosecond pulses. *Nanophotonics* **11**, 3081-3091 (2022).
102. Liu, Y. H. et al. λ/12 super resolution achieved in maskless optical projection nanolithography for efficient cross-scale patterning. *Nano Letters* **21**, 3915-3921 (2021).
103. Lim, M. P. et al. Augmenting mask-based lithography with direct laser writing to increase resolution and speed. *Optics Express* **26**, 7085-7090 (2018).
104. Schmidt, J. et al. Multiscale ceramic components from preceramic polymers by hybridization of vat polymerization-based technologies. *Additive Manufacturing* **30**, 100913 (2019).
105. Tan, M. Y. et al. Cross-scale and cross-precision structures/systems fabricated by high-efficiency and low-cost hybrid 3D printing technology. *Additive Manufacturing* **59**, 103169 (2022).
106. Tan, M. Y. et al. Microflow multi-layer diffraction optical element processed by hybrid manufacturing technology. *Optics Express* **30**, 24689-24702 (2022).
107. Lee, K. S. et al. Advances in 3D nano/microfabrication using two-photon initiated polymerization. *Progress in Polymer Science* **33**, 631-681 (2008).
108. Sarhadi, A., Hattel, J. H. & Hansen, H. N. Three-dimensional modeling of glass lens molding. *International Journal of Applied Glass Science* **6**, 182-195 (2015).
109. Zhou, X. Q., Hou, Y. H. & Lin, J. Q. A review on the processing accuracy of two-photon polymerization. *AIP Advances* **5**, 030701 (2015).
110. Zheng, X. et al. An adaptive direct slicing method based on tilted voxel of two-photon polymerization. *The International Journal of Advanced Manufacturing Technology* **96**, 521-530 (2018).
111. Wu, D. et al. High numerical aperture microlens arrays of close packing. *Applied Physics Letters* **97**, 031109 (2010).
112. Park, S. H. et al. Subregional slicing method to increase three-dimensional nanofabrication efficiency in two-photon polymerization. *Applied Physics Letters* **87**, 154108 (2005).
113. Jing, X. et al. Adaptive slicing method for three-dimensional microstructures with free-form surfaces in two photon polymerization microfabrication. *Nano* **14**, 1950006 (2019).
114. Malinauskas, M. et al. Femtosecond laser polymerization of hybrid/integrated micro-optical elements and their characterization. *Journal of Optics* **12**, 124010 (2010).
115. Guo, R. et al. Micro lens fabrication by means of femtosecond two photon photopolymerization. *Optics Express* **14**, 810-816 (2006).
116. Liao, C. Y. et al. Two-dimensional slicing method to speed up the fabrication of micro-objects based on two-photon polymerization. *Applied Physics Letters* **91**, 033108 (2007).
117. Yang, D. Y. et al. Ultraprecise microreproduction of a three-dimensional artistic sculpture by multipath scanning method in two-photon photopolymerization. *Applied Physics Letters* **90**, 013113 (2007).
118. Geisler, E. , Lecompère, M. & Soppera, O. 3D printing of optical materials by processes based on photopolymerization: materials, technologies, and recent advances. *Photonics Research* **10**, 06001344 (2022).
119. Zhao, Y. Y. et al. Three-dimensional Luneburg lens at optical frequencies. *Laser & Photonics Reviews* **10**, 665-672 (2016).
120. Sartison, M. 3D printed micro-optics for quantum technology: Optimised coupling of single quantum dot emission into a single-mode fibre. *Light: Advanced Manufacturing* **2**, 6 (2021).
121. Schmid, M. et al. 3D printed hybrid refractive/diffractive achromat and apochromat for the visible wavelength range. *Optics Letters* **46**, 2485-2488 (2021).
122. Tian, Z. N. et al. Mirror-rotation-symmetrical single-focus spiral zone

plates. *Optics Letters* **43**, 3116-3119 (2018).
123. Baldacchini, T. et al. Acrylic-based resin with favorable properties for three-dimensional two-photon polymerization. *Journal of Applied Physics* **95**, 6072-6076 (2004).
124. Cao, J. J. et al. Bioinspired Zoom Compound Eyes Enable Variable-Focus Imaging. *ACS Applied Materials & Interfaces* **12**, 10107-10117 (2020).
125. Ma, Z. C. et al. Smart compound eyes enable tunable imaging. *Advanced Functional Materials* **29**, 1903340 (2019).
126. Sun, Y. L. et al. Dynamically tunable protein microlenses. *Angewandte Chemie International Edition* **51**, 1558-1562 (2012).
127. Kotz, F. et al. Two-photon polymerization of nanocomposites for the fabrication of transparent fused silica glass microstructures. *Advanced Materials* **33**, 2006341 (2021).
128. Wen, X. W. et al. 3D-printed silica with nanoscale resolution. *Nature Materials* **20**, 1506-1511 (2021).
129. Zhang, H. et al. Overview of 3D-printed silica glass. *Micromachines* **13**, 81 (2022).
130. Hong, Z. H. et al. Three-dimensional printing of glass micro-optics. *Optica* **8**, 904-910 (2021).
131. Doualle, T. , André, J. C. & Gallais, L. 3D printing of silica glass through a multiphoton polymerization process. *Optics Letters* **46**, 364-367 (2021).
132. Kotz, F. et al. Liquid glass: a facile soft replication method for structuring glass. *Advanced Materials* **28**, 4646-4650 (2016).
133. Gonzalez-Hernandez, D. et al. Laser 3D printing of inorganic free-form micro-optics. *Photonics* **8**, 577 (2021).
134. Xiong, W. et al. Simultaneous additive and subtractive three-dimensional nanofabrication using integrated two-photon polymerization and multiphoton ablation. *Light:Science & Applications* **1**, e6 (2012).
135. Zhou, G. Y., Ventura, M. J. & Gu, M. Photonic bandgap properties of void-based body-centered-cubic photonic crystals in polymer. *Optics Express* **13**, 4390-4395 (2005).
136. Yong, J. L. et al. Rapid fabrication of large-area concave microlens arrays on PDMS by a femtosecond laser. *ACS Applied Materials & Interfaces* **5**, 9382-9385 (2013).
137. Liu, X. F., Yang, Y. T. & Qiu, J. R. Emerging techniques for customized fabrication of glass. *Journal of Non-Crystalline Solids:X* **15**, 100114 (2022).
138. Kotz, F. et al. Glassomer-processing fused silica glass like a polymer. *Advanced Materials* **30**, 1707100 (2018).
139. Bhanvadia, A. A. et al. High-resolution stereolithography using a static liquid constrained interface. *Communications Materials* **2**, 41 (2021).
140. Kotz, F. et al. Three-dimensional printing of transparent fused silica glass. *Nature* **544**, 337-339 (2017).
141. Balčas, G. et al. Fabrication of glass-ceramic 3D micro-optics by combining laser lithography and calcination. *Advanced Functional Materials* **33**, 2215230 (2023).
142. Lin, G. et al. Glass-ceramics with embedded gallium/aluminum nanoalloys formed by heat treatment and femtosecond laser irradiation. *Journal of the American Ceramic Society* **95**, 776-781 (2012).
143. Gailevičius, D. et al. Additive-manufacturing of 3D glass-ceramics down to nanoscale resolution. *Nanoscale Horizons* **4**, 647-651 (2019).
144. Cooperstein, I. et al. Additive manufacturing of transparent silica glass from solutions. *ACS Applied Materials & Interfaces* **10**, 18879-18885 (2018).
145. Bauer, J., Crook, C. & Baldacchini, T. A sinterless, low-temperature route to 3D print nanoscale optical-grade glass. *Science* **380**, 960-966 (2023).
146. Fang, G. et al. Femtosecond laser direct writing of 3D silica-like microstructure from hybrid epoxy cyclohexyl POSS. *Advanced Materials Technologies* **3**, 1700271 (2018).
147. Huang, P. H. et al. Three-dimensional printing of silica glass with sub-micrometer resolution. *Nature Communications* **14**, 3305 (2023).
148. Jin, F. et al. λ/30 inorganic features achieved by multi-photon 3D lithography. *Nature Communications* **13**, 1357 (2022).
149. Ma, Z. C. et al. Femtosecond-laser direct writing of metallic micro/nanostructures: from fabrication strategies to future applications. *Small Methods* **2**, 1700413 (2018).
150. Low, M. J. et al. Laser-induced reduced-graphene-oxide micro-optics patterned by femtosecond laser direct writing. *Applied Surface Science* **526**, 146647 (2020).
151. Low, M. J. et al. Refractive-diffractive hybrid optics array: comparative analysis of simulation and experiments. *Journal of Optics* **24**, 055401 (2022).
152. Zhang, Y. L. et al. Electro-responsive actuators based on graphene. *The Innovation* **2**, 100168 (2021).
153. Jiang, L. J. et al. Femtosecond laser direct writing in transparent materials based on nonlinear absorption. *MRS Bulletin* **41**, 975-983 (2016).
154. Li, Q. S. et al. Phase-type fresnel zone plate with multi-wavelength imaging embedded in fluoroaluminate glass fabricated via ultraviolet femtosecond laser lithography. *Micromachines* **12**, 1362 (2021).
155. Li, Q. K. et al. Multilevel phase-type diffractive lens embedded in sapphire. *Optics Letters* **42**, 3832-3835 (2017).
156. Liu, X. Q. et al. Dry-etching-assisted femtosecond laser machining. *Laser & Photonics Reviews* **11**, 1600115 (2017).
157. Deng, Z. F. et al. Fabrication of large-area concave microlens array on silicon by femtosecond laser micromachining. *Optics Letters* **40**, 1928-1931 (2015).
158. Pan, A. et al. Fabrication of concave spherical microlenses on silicon by femtosecond laser irradiation and mixed acid etching. *Optics Express* **22**, 15245-15250 (2014).
159. Krol, D. M. Femtosecond laser modification of glass. *Journal of Non-Crystalline Solids* **354**, 416-424 (2008).
160. Trusovas, R. et al. Recent advances in laser utilization in the chemical modification of graphene oxide and its applications. *Advanced Optical Materials* **4**, 37-65 (2016).
161. Tan, D. Z. et al. Femtosecond laser induced phenomena in transparent solid materials: Fundamentals and applications. *Progress in Materials Science* **76**, 154-228 (2016).
162. Lin, D. M. et al. Dielectric gradient metasurface optical elements. *Science* **345**, 298-302 (2014).
163. Khorasaninejad, M. et al. Achromatic metasurface lens at telecommunication wavelengths. *Nano Letters* **15**, 5358-5362 (2015).
164. Zhou, J. D. et al. A library of atomically thin metal chalcogenides. *Nature* **556**, 355-359 (2018).
165. Cong, S. et al. Surface enhanced raman scattering revealed by interfacial charge-transfer transitions. *The Innovation* **1**, 100051 (2020).
166. Lin, H. et al. Diffraction-limited imaging with monolayer 2D material-based ultrathin flat lenses. *Light:Science & Applications* **9**, 137 (2020).
167. West, P. R. et al. All-dielectric subwavelength metasurface focusing lens. *Optics Express* **22**, 26212-26221 (2014).
168. Kang, S., Vora, K. & Mazur, E. One-step direct-laser metal writing of sub-100 nm 3D silver nanostructures in a gelatin matrix. *Nanotechnology* **26**, 121001 (2015).
169. Liu, X. J. et al. Recent advances in stimuli-responsive shape-morphing hydrogels. *Advanced Functional Materials* **32**, 2203323 (2022).
170. Han, F. et al. Three-dimensional nanofabrication via ultrafast laser patterning and kinetically regulated material assembly. *Science* **378**, 1325-1331 (2022).
171. Malinauskas, M. et al. A femtosecond laser-induced two-photon photopolymerization technique for structuring microlenses. *Journal of Optics* **12**, 035204 (2010).
172. Berglund, G. D. & Tkaczyk, T. S. Fabrication of optical components

using a consumer-grade lithographic printer. *Optics Express* **27**, 30405-30420 (2019).
173. Liu, M. N. et al. Etching-assisted femtosecond laser microfabrication. *Chinese Physics B* **27**, 094212 (2018).
174. Kim, J. Y. et al. Directly fabricated multi-scale microlens arrays on a hydrophobic flat surface by a simple ink-jet printing technique. *Journal of Materials Chemistry* **22**, 3053-3058 (2012).
175. Zhou, F. et al. Additive manufacturing of a 3D terahertz gradient-refractive index lens. *Advanced Optical Materials* **4**, 1034-1040 (2016).
176. Xu, J. J. et al. High curvature concave–convex microlens. *IEEE Photonics Technology Letters* **27**, 2465-2468 (2015).
177. Chen, Z. H. et al. Variable focus convex microlens array on K9 glass substrate based on femtosecond laser processing and hot embossing lithography. *Optics Letters* **47**, 22-25 (2022).
178. Wu, D. et al. 100% Fill-factor aspheric microlens arrays (AMLA) with Sub-20-nm precision. *IEEE Photonics Technology Letters* **21**, 1535-1537 (2009).
179. Schmid, M. D. et al. 3D direct laser writing of highly absorptive photoresist for miniature optical apertures. *Advanced Functional Materials* **33**, 2211159 (2023).
180. Aieta, F. et al. Multiwavelength achromatic metasurfaces by dispersive phase compensation. *Science* **347**, 1342-1345 (2015).
181. Bianchi, S. et al. Focusing and imaging with increased numerical apertures through multimode fibers with micro-fabricated optics. *Optics Letters* **38**, 4935-4938 (2013).
182. Zhang, B. et al. Femtosecond laser modification of 6H–SiC crystals for waveguide devices. *Applied Physics Letters* **116**, 111903 (2020).
183. Atwater, J. H. et al. Microphotonic parabolic light directors fabricated by two-photon lithography. *Applied Physics Letters* **99**, 151113 (2011).
184. Zheng, Q. et al. Rapid prototyping of a dammann grating in DMD-based maskless lithography. *IEEE Photonics Journal* **11**, 2400410 (2019).
185. Sanli, U. T. et al. 3D nanoprinted plastic kinoform X-Ray optics. *Advanced Materials* **30**, 1802503 (2018).
186. Huang, Y. et al. Multi-value phase grating fabrication using direct laser writing for generating a two-dimensional focal spot array. *Journal of Optics* **24**, 055601 (2022).
187. Huang, L. et al. Technology of static oblique lithography used to improve the fidelity of lithography pattern based on DMD projection lithography. *Optics & Laser Technology* **157**, 108666 (2023).
188. Hu, Z. Y. et al. Broad-bandwidth micro-diffractive optical elements. *Laser & Photonics Reviews* **16**, 2100537 (2022).
189. Mohacsi, I. et al. Fabrication and characterization of high-efficiency double-sided blazed x-ray optics. *Optics Letters* **41**, 281-284 (2016).
190. Wu, D. et al. High efficiency multilevel phase-type fractal zone plates. *Optics Letters* **33**, 2913-2915 (2008).
191. Sun, Y. L. et al. Protein-based soft micro-optics fabricated by femtosecond laser direct writing. *Light:Science & Applications* **3**, e129 (2014).
192. Xiong, Z. et al. Femtosecond Laser Densification of Hydrogels to Generate Customized Volume Diffractive Gratings. *ACS Applied Materials & Interfaces* **14**, 29377-29385 (2022).
193. Pan, M. Y. et al. Dielectric metalens for miniaturized imaging systems: progress and challenges. *Light:Science & Applications* **11**, 195 (2022).
194. Hadibrata, W. et al. Inverse design and 3D printing of a metalens on an optical fiber tip for direct laser lithography. *Nano Letters* **21**, 2422-2428 (2021).
195. Balli, F. et al. A hybrid achromatic metalens. *Nature Communications* **11**, 3892 (2020).
196. Wei, S. B. et al. A varifocal graphene metalens for broadband zoom imaging covering the entire visible region. *ACS Nano* **15**, 4769-4776 (2021).
197. Schlickriede, C. et al. Imaging through nonlinear metalens using second harmonic generation. *Advanced Materials* **30**, 1703843 (2018).
198. Paniagua-Domínguez, R. et al. A metalens with a near-unity numerical aperture. *Nano Letters* **18**, 2124-2132 (2018).
199. Faklis, D. & Morris, G. M. Spectral properties of multiorder diffractive lenses. *Applied Optics* **34**, 2462-2468 (1995).
200. Nair, S. P. et al. 3D printing mesoscale optical components with a low-cost resin printer integrated with a fiber-optic taper. *ACS Photonics* **9**, 2024-2031 (2022).
201. Sun, Y. L. et al. Tunable protein harmonic diffractive micro-optical elements. *Optics Letters* **37**, 2973-2975 (2012).
202. Hua, J. G. et al. Centimeter-sized aplanatic hybrid diffractive-refractive lens. *IEEE Photonics Technology Letters* **31**, 3-6 (2019).
203. Tian, Z. N. et al. Hybrid refractive–diffractive optical vortex microlens. *IEEE Photonics Technology Letters* **28**, 2299-2302 (2016).
204. Gissibl, T. et al. Sub-micrometre accurate free-form optics by three-dimensional printing on single-mode fibres. *Nature Communications* **7**, 11763 (2016).
205. Li, J. W. et al. 3D-printed micro lens-in-lens for in vivo multimodal microendoscopy. *Small* **18**, 2107032 (2022).
206. Zhou, Z. T. et al. The use of functionalized silk fibroin films as a platform for optical diffraction-based sensing applications. *Advanced Materials* **29**, 1605471 (2017).
207. Keum, D. et al. Xenos peckii vision inspires an ultrathin digital camera. *Light:Science & Applications* **7**, 80 (2018).
208. Wang, D. Y. et al. 3D printing challenges in enabling rapid response to public health emergencies. *Innovation* **1**, 100056 (2020).
209. Rekštytė, S., Malinauskas, M. & Juodkazis, S. Three-dimensional laser micro-sculpturing of silicone: towards bio-compatible scaffolds. *Optics Express* **21**, 17028-17041 (2013).
210. Hernandez-Cedillo, L. et al. Peculiarities of integrating mechanical valves in microfluidic channels using direct laser writing. *Applied Bionics and Biomechanics* **2022**, 9411024 (2022).
211. Nair, S. P. et al. 3D printed fiber sockets for plug and play micro-optics. *International Journal of Extreme Manufacturing* **3**, 015301 (2020).
212. Tan, M. Y. et al. Double-sided femtosecond 3D printing technology based on a specific mask. *Optics and Lasers in Engineering* **161**, 107328 (2023).
213. Xiong, C. et al. Optical fiber integrated functional micro-/nanostructure induced by two-photon polymerization. *Frontiers in Materials* **7**, 586496 (2020).
214. Sivankutty, S. et al. Miniature 120-beam coherent combiner with 3D-printed optics for multicore fiber-based endoscopy. *Optics Letters* **46**, 4968-4971 (2021).
215. Gissibl, T. et al. Two-photon direct laser writing of ultracompact multi-lens objectives. *Nature Photonics* **10**, 554-560 (2016).
216. Li, B. Z. et al. Femtosecond laser 3D printed micro objective lens for ultrathin fiber endoscope. *Fundamental Research* (in the press).
217. Kiekens, K. C. & Barton, J. K. 3D printed lens for depth of field imaging. *OSA Continuum* **2**, 3019-3025 (2019).
218. Thiele, S. et al. 3D printed stacked diffractive microlenses. *Optics Express* **27**, 35621-35630 (2019).
219. Galvez, D. et al. Characterizing close-focus lenses for microendoscopy. *Journal of Optical Microsystems* **3**, 011003 (2023).
220. Jin, G. X. et al. Femtosecond laser fabrication of 3D templates for mass production of artificial compound eyes. *Nanotechnology and Precision Engineering* **2**, 110-117 (2019).
221. Thiele, S. et al. 3D-printed eagle eye: compound microlens system for foveated imaging. *Science Advances* **3**, e1602655 (2017).
222. Li, J. W. et al. Ultrathin monolithic 3D printed optical coherence tomography endoscopy for preclinical and clinical use. *Light:Science & Applications* **9**, 124 (2020).
223. Hong, Z. H. et al. Bio-inspired compact, high-resolution snapshot

hyperspectral imaging system with 3D printed glass lightguide array. *Advanced Optical Materials* **11**, 2300156 (2023).
224. Hu, Y. L. et al. All-glass 3D optofluidic microchip with built-in tunable microlens fabricated by femtosecond laser-assisted etching. *Advanced Optical Materials* **6**, 1701299 (2018).
225. Wu, D. et al. Facile creation of hierarchical PDMS microstructures with extreme underwater superoleophobicity for anti-oil application in microfluidic channels. *Lab on a Chip* **11**, 3873-3879 (2011).
226. Wu, D. et al. Femtosecond laser rapid prototyping of nanoshells and suspending components towards microfluidic devices. *Lab on a Chip* **9**, 2391-2394 (2009).
227. Lu, D. X. et al. Solvent-tunable PDMS microlens fabricated by femtosecond laser direct writing. *Journal of Materials Chemistry C* **3**, 1751-1756 (2015).
228. Zhao, X. Y. et al. Tunable optofluidic microbubble lens. *Optics Express* **30**, 8317-8329 (2022).
229. Wu, D. et al. In-channel integration of designable microoptical devices using flat scaffold-supported femtosecond-laser microfabrication for coupling-free optofluidic cell counting. *Light:Science & Applications* **4**, e228 (2015).
230. Wu, D. et al. Hybrid femtosecond laser microfabrication to achieve true 3D glass/polymer composite biochips with multiscale features and high performance: the concept of ship-in-a-bottle biochip. *Laser & Photonics Reviews* **8**, 458-467 (2014).
231. Royon, A. et al. Silver clusters embedded in glass as a perennial high capacity optical recording medium. *Advanced Materials* **22**, 5282-5286 (2010).
232. Zhang, J. Y. et al. Seemingly unlimited lifetime data storage in nanostructured glass. *Physical Review Letters* **112**, 033901 (2014).
233. Chan, J. W. et al. Fluorescence spectroscopy of color centers generated in phosphate glasses after exposure to femtosecond laser pulses. *Journal of the American Ceramic Society* **85**, 1037-1040 (2004).
234. Huang, X. J. et al. Reversible 3D laser printing of perovskite quantum dots inside a transparent medium. *Nature Photonics* **14**, 82-88 (2020).
235. Weber, K. et al. Single mode fiber based delivery of OAM light by 3D direct laser writing. *Optics Express* **25**, 19672-19679 (2017).
236. Liu, Z. Y. et al. A beam homogenizer for digital micromirror device lithography system based on random freeform microlenses. *Optics Communications* **443**, 211-215 (2019).
237. Zhang, H. et al. Random silica-glass microlens arrays based on the molding technology of photocurable nanocomposites. *ACS Applied Materials & Interfaces* **15**, 19230-19240 (2023).
238. Gissibl, T., Schmid, M. & Giessen, H. Spatial beam intensity shaping using phase masks on single-mode optical fibers fabricated by femtosecond direct laser writing. *Optica* **3**, 448-451 (2016).
239. Thiele, S. et al. Ultra-compact on-chip LED collimation optics by 3D femtosecond direct laser writing. *Optics Letters* **41**, 3029-3032 (2016).
240. Hamadani, B. H. , Seppala, J. & Zarobila, C. 3D printed optical concentrators for LED arrays. *OSA Continuum* **3**, 2022-2035 (2020).
241. Lightman, S. et al. Shaping of light beams by 3D direct laser writing on facets of nonlinear crystals. *Optics Letters* **40**, 4460-4463 (2015).
242. Jung, N. T. et al. 3D quantum dot-lens fabricated by stereolithographic printing with in-situ UV curing for lighting and displays. *Composites Part B: Engineering* **226**, 109350 (2021).
243. Fischbach, S. et al. Single quantum dot with microlens and 3D-printed micro-objective as integrated bright single-photon source. *ACS Photonics* **4**, 1327-1332 (2017).
244. Schäffner, D. et al. Arrays of individually controllable optical tweezers based on 3D-printed microlens arrays. *Optics Express* **28**, 8640-8645 (2020).
245. Lightman, S. et al. Miniature wide-spectrum mode sorter for vortex beams produced by 3D laser printing. *Optica* **4**, 605-610 (2017).
246. Yu, S. L. et al. On-chip optical tweezers based on freeform optics. *Optica* **8**, 409-414 (2021).
247. Asadollahbaik, A. et al. Highly efficient dual-fiber optical trapping with 3D printed diffractive fresnel lenses. *ACS Photonics* **7**, 88-97 (2020).
248. Xu, Y. L. et al. 3D-printed facet-attached microlenses for advanced photonic system assembly. *Light: Advanced Manufacturing* **4**, 3 (2023).
249. Toulouse, A. et al. 3D-printed miniature spectrometer for the visible range with a 100 × 100 μm^2 footprint. *Light: Advanced Manufacturing* **2**, 2 (2021).
250. Hong, Z. H. et al. High-precision printing of complex glass imaging optics with precondensed liquid silica resin. *Advanced Science* **9**, 2105595 (2022).
251. Flamini, F. et al. Thermally reconfigurable quantum photonic circuits at telecom wavelength by femtosecond laser micromachining. *Light:Science & Applications* **4**, e354 (2015).
252. Zhang, X. L. et al. Non-Abelian braiding on photonic chips. *Nature Photonics* **16**, 390-395 (2022).
253. Li, M. et al. On-chip path encoded photonic quantum Toffoli gate. *Photonics Research* **10**, 1533-1542 (2022).
254. Mader, M. et al. High-throughput injection molding of transparent fused silica glass. *Science* **372**, 182-186 (2021).
255. Zhang, D. et al. Highly efficient phosphor-glass composites by pressureless sintering. *Nature Communications* **11**, 2805 (2020).
256. Xu, S. et al. High-efficiency fabrication of geometric phase elements by femtosecond-laser direct writing. *Nanomaterials* **10**, 1737 (2020).
257. De Marzi, A. et al. Hybrid additive manufacturing for the fabrication of freeform transparent silica glass components. *Additive Manufacturing* **54**, 102727 (2022).
258. Feng, J. W. et al. Triply periodic minimal surface (TPMS) porous structures: from multi-scale design, precise additive manufacturing to multidisciplinary applications. *International Journal of Extreme Manufacturing* **4**, 022001 (2022).
259. Toombs, J. T. et al. Volumetric additive manufacturing of silica glass with microscale computed axial lithography. *Science* **376**, 308-312 (2022).
260. Kunwar, P. et al. Hybrid laser printing of 3D, multiscale, multimaterial hydrogel structures. *Advanced Optical Materials* **7**, 1900656 (2019).
261. Kang, W. J. , Hong, Z. H. & Liang, R. G. 3D printing optics with hybrid material. *Applied Optics* **60**, 1809-1813 (2021).
262. Yang, L. et al. Multi-material multi-photon 3D laser micro- and nanoprinting. *Light:Advanced Manufacturing* **2**, 17 (2021).
263. Ouyang, W. Q. et al. Ultrafast 3D nanofabrication via digital holography. *Nature Communications* **14**, 1716 (2023).
264. Maier, P. et al. 3D-printed facet-attached optical elements for connecting VCSEL and photodiodes to fiber arrays and multi-core fibers. *Optics Express* **30**, 46602-46625 (2022).
265. Singer, S. et al. 3D-printed facet-attached optical elements for beam shaping in optical phased arrays. *Optics Express* **30**, 46564-46574 (2022).
266. Li, Q. Y. et al. Direct 3D-printing of microlens on single mode polarization-stable VCSEL chip for miniaturized optical spectroscopy. *Journal of Optical Microsystems* **3**, 033501 (2023).